

1 **Author's Response**

2 **“Occurrence and characteristics of mesoscale eddies in the tropical northeast Atlantic**  
3 **Ocean”**

4 **Florian Schuette, Peter Brandt and Johannes Karstensen**

5 fschuette@geomar.de

6

7

8 Dear Editor,

9 We would like to thank you for the positive evaluation of our manuscript, the constructive  
10 criticism and the very careful corrections and suggestions, which surely helped to improve the  
11 manuscript. On the next pages we will answer point by point to the remarks of the reviewers  
12 and how we intend to address their concerns in the manuscript. Below, comments by the  
13 reviewers are marked italic and our response as normal text. At the end we included a  
14 marked-up manuscript version.

15

16

17 **Anonymous Referee #1**

18 *The paper presents an appropriate overview of eddy properties off the west African up-*  
19 *welling (TANWA region) and of their contribution to transports. It uses most of the data of the*  
20 *upper ocean available, either in situ or satellite-based, and nicely synthesizes the results. The*  
21 *methodology both for identifying eddies, tracking them or establishing their properties is*  
22 *appropriate. The introduction gives a fine state-of-the-art review, and the discussion/*  
23 *conclusion sections presents a fine analysis of the relevance of the results and of possible*  
24 *limitations of the approach.*

25 Thank you very much for this evaluation.

26

1 *What follows are some minor comments/queries:*

2 **Data and methods:**

3 *Right choice of satellite data products. Among the data, glider data collected in this region*  
4 *have not been used. Is it because of insufficient vertical reach of the glider CTD data? (maybe*  
5 *not before end 2013?).*

6  
7 - Before the end of 2013 we only had two glider missions in the TANWA (2010 and 2013)  
8 that possibly could use in the present eddy study. We checked the glider data on potential  
9 eddy crossings and found only few profiles that could be used, but overall do not help to  
10 improve the eddy statistics significantly. Thus we decided not to use glider data here.  
11 However, for future studies glider data is getting interesting due to the intensification of glider  
12 deployments in the TANWA during the last years in the project AWA/Eddy-Hunt (see also  
13 special issue in Biogeosciences: [http://www.biogeosciences.net/special\\_issue213.html](http://www.biogeosciences.net/special_issue213.html)).

14  
15 *Among the Argo data, 40% rejection with the three criteria chosen seemed particularly high:*  
16 *which of the criteria used explains that in this region?*

17  
18 - The Argo float data marked with quality category 1 still had several issues, which led to the  
19 rejection of the relatively large number of profiles for the present study. From original 2906  
20 profiles in the TANWA we delete 886 profiles (31%): 52 profiles were deleted because they  
21 have no data between 0 and 10 m depth; 31 profiles were deleted because they have less than  
22 4 data points in the upper 200 m; 139 profiles were deleted because they do not reach down to  
23 1000 m. The remaining 664 profiles were deleted because either the temperature, salinity or  
24 pressure measurement was not existent, the pressure was not continuous or temperature or  
25 salinity measurements were obviously wrong for that region (temperature > 40°C and 30 <  
26 salinity > 40). This additional information of how many profiles are rejected due to the  
27 different criteria's is now added to the manuscript (page 3051, line 13-17):

28  
29 „In the following, we give the criteria applied to the Argo float profiles and in brackets the  
30 percentage, to which the criteria were fulfilled. Selected profiles must i) include data between  
31 0 and 10 m depth (98.2%), ii) have at least 4 data points in the upper 200 m (98.8%), iii) reach  
32 down to 1000 m depths (95%), iv) continuous and consistent temperature, salinity and  
33 pressure data (78%). This procedure reduced the number of profiles by around 30% to 2022  
34 Argo float profiles for the TANWA.“

1  
2  
3  
4  
5  
6  
7  
8  
9  
10  
11  
12  
13  
14  
15  
16  
17  
18  
19  
20  
21  
22  
23  
24  
25  
26  
27  
28  
29  
30  
31

*In CVOO mooring profiles, the reference profile is chosen before the eddy passage. Any reason for not also taking into account profiles collected afterwards?*

- We thought that the profile before the eddy passage is very likely not affected by the eddy, while the profile after the eddy passage could include contributions from the eddy core mixed with the surroundings. But we checked now diverse profiles before and after the eddy passage and could not find a systematic difference. Thus, we agree with the reviewer and conclude that it is not relevant if a reference profile is taken before or after an eddy.

*Bottom page 3053, line 17-19: not completely clear. Is it that for each profile inside an eddy, one checks whether there are reference profiles outside of the eddy filling the criteria and then estimate (or not) an anomaly. . .*

- Yes, it is exactly what we have done. For every profile inside of an eddy we searched for a reference profile outside of an eddy to compute an anomaly. This reference profile should be at maximum 120 km apart of the eddy center (not within another eddy) and  $\pm 25$  days apart from the time the profile inside of the eddy were taken. If no reference profile is fulfilling these criteria, an anomaly cannot be derived. To clarify this we changed page 3052 line 15 to 20 from:

“Here we are interested in the anomalous water mass characteristic inside the eddy compared to the surrounding water. Anomaly profiles of potential temperature,  $\theta$ , salinity, S, and potential density,  $\sigma_\theta$ , were derived as the difference of the profiles inside and reference profiles outside of an eddy. Profiles outside of eddies are required to be taken within a maximum distance of 120 km from the eddy centre and at maximum  $\pm 25$  days apart from the time the profile inside of the eddy were taken (Figure 4). For 176 profiles out of the 1174 profiles inside of eddies no reference profile could be found fulfilling these criteria. In total 587 anomaly profiles for anticyclones/ACMEs and 411 anomaly profiles for cyclones were derived.”

**Results and Discussion**

1 *The average eddy-radius is 56 km, so it is rather close to the resolution in the AVISO*  
2 *products that are used to estimate the eddy statistics (size, velocity). What is the implication*  
3 *on these statistics?*

4 - As correctly mentioned by the reviewer the AVISO SLA products cannot resolve eddies  
5 with radii smaller than 45-50 km and, consequently, no eddies with radii smaller than 45 km  
6 were included in our database. The occurrence of eddies decreases rapidly with increasing  
7 eddy radius and eddies with radii between 45 – 60 km that are close to the resolution limit of  
8 the AVISO product dominate the eddy statistics. Thus, the given number of eddies and  
9 corresponding eddy fluxes must be seen as a lower limit and would increase if accounting for  
10 smaller eddies. We include a corresponding sentence in the manuscript at page 3056, line 11:

11 “Note, that the given number of eddies must be seen as lower limit due to the coarse  
12 resolution of the satellite products.”

13 *I understand that the uncertainties in tracking due to errors in mappings (insufficient*  
14 *altimetric coverage) requires to check whether same eddy reemerges a while after. I did not*  
15 *fully understand what is the criterion used to identify a same structure after a tracking*  
16 *interruption.*

17 - The insufficient explanation of the tracking algorithm was also noted by referee #2. We  
18 rephrased this paragraph and added additional information to improve its structure, both  
19 hopefully clarifying the description of the applied algorithms. We added the paragraph at page  
20 3050 line 3-11:

21 “When applying the two different eddy detection methods to the SLA data from the TANWA  
22 region, we used the same eddy detection thresholds for both methods, i.e. a feature only  
23 counts as an eddy, if its radius is larger than 45 km and it is detectable for a period of more  
24 than 7 days. Note, as the identified eddy areas are rarely circular we used the circle-equivalent  
25 of the area of the detected features to estimate the radius. For eddy tracking both eddy  
26 detection methods use the same tracking algorithm. An eddy trajectory was calculated if an  
27 eddy with the same polarity was found at least in 7 consecutive SLA maps (corresponding to  
28 one weeks) within a search radius of up to 50 km. Due to e.g. errors in SLA mappings  
29 (insufficient altimetric coverage) an eddy could vanish and reemerge after a while. Therefore  
30 we searched in 14 consecutive SLA maps (corresponding to 2 weeks) in a search radius of up  
31 to 100 km after an eddy disappearance, if eddies with the same polarity reemerges. If more



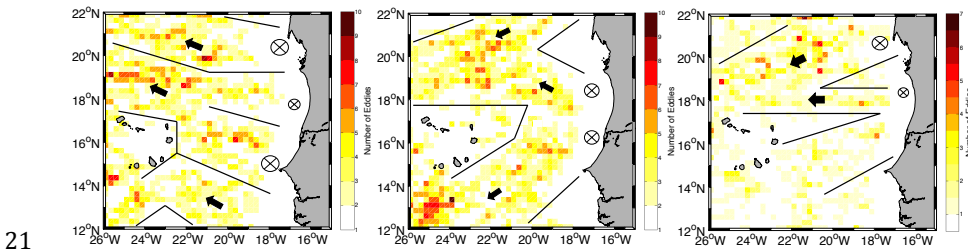
1 than one eddy with the same polarity emerge within the search radius, we defined the  
2 following similarity parameter to discriminate between the eddies:

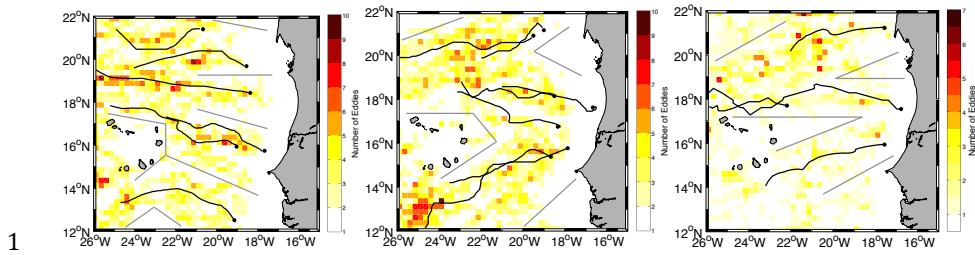
3  
4 
$$X = \sqrt{\left(\frac{\text{distance}}{100}\right)^2 + \left(\frac{\Delta \text{radius}}{\text{radius}_0}\right)^2 + \left(\frac{\Delta \text{vorticity}}{\text{vorticity}_0}\right)^2 + \left(\frac{\Delta \text{EKE}}{\text{EKE}_0}\right)^2}, \quad (1)$$

5 which include four terms including the distance and the difference of the two radii, mean  
6 vorticities and mean EKE of the eddies.  $\text{Radius}_0$ ,  $\text{vorticity}_0$  and  $\text{EKE}_0$  are the mean radius,  
7 vorticity and EKE of all identified eddies in TANWA. The eddy with the smallest X is  
8 selected to be the same eddy.”

9 *3.2 formation and propagation (pages 3058-3059). Very interesting and informative sections.*  
10 *On the other hand, the arrows and eddy corridors delineated on figures 8 (right panels) are*  
11 *rather schematic. Is there a way to be more quantitative there. At least, it should be possible*  
12 *to add average speed (both zonal and meridional) as well as its rms for these different*  
13 *'average' vectors (and each eddy type). For ACME, however, statistics might not be that*  
14 *relevant. Seems that they are mostly in the north?*

15 - Referee #2 also noted the rather schematic presentation of the eddy propagation in figure 8.  
16 We decided to add trajectories of long-lived eddies exemplarily showing the eddy propagation  
17 direction and pathways (see figure 1). The satellite statistics indicate that long-lived ACMEs  
18 occur mostly in the northern part of TANWA, but recent in-situ observations found ACME  
19 structures in surprisingly high numbers and in a wide area from about 5°N to 20°N east of  
20 30°W in the tropical Northeast Atlantic Ocean (for more details see Schütte et al. 2016).





1  
2 **Figure 1:** Upper row old figures: Total number of eddies detected in  $1/6^\circ \times 1/6^\circ$  boxes for  
3 cyclones, anticyclones and ACMEs. Only eddies are counted with a lifetime larger than 35  
4 days. Main eddy propagation corridors are indicated by solid black lines and thick black  
5 arrows, main generation spots by circles with crosses. Lower row new figures: Total number  
6 of eddies detected in  $1/6^\circ \times 1/6^\circ$  boxes for cyclones, anticyclones and ACMEs. Only eddies  
7 are counted with a lifetime larger than 35 days. Main eddy propagation corridors are indicated  
8 by solid grey lines and selected trajectories of long-lived eddies. The dots mark the starting  
9 point of the eddy trajectories.

10 *p.3059-3060 interesting strong seasonal dependency on cyclone formation that is correctly*  
11 *identified and analyzed. I see it much less with anticyclones (except after removing ACME),*  
12 *and not so sure that the July isolated peak is so relevant (or at least, this should be further*  
13 *argued; as one could as well state the maximum at the end of the year...).*

14 - We agree with the reviewers comment and included one sentence at page 3060 line 12-13 to  
15 mention the maximum of anticyclone formation at the end of the year:

16 “While the maximum formation of cyclones occurs in June during the acceleration phase of  
17 the MC, the seasonality of anticyclone formation is not as distinct with weaker maxima in  
18 July and at the end of the year.”

19 *Obviously, ACME have a formation peak in spring, during the core upwelling season. Is it the*  
20 *influence of the undercurrent water, which would also explain why they have such a strong*  
21 *SACW signature?*

22 - Yes, we think that the instability of the poleward undercurrent (PUC), which is strongest  
23 during the core upwelling season (spring), are involved in the formation of ACMEs (e.g. as  
24 suggested by D’Asaro 1988). The PUC with its core depth at around 100 m depth transports  
25 SACW northward, which could explain the strong SACW signature of ACMEs. Hence water

1 mass anomalies and depth range of ACME cores coincide with the PUC. However, we have  
2 no observational evidence of the instability process. That is why we are not discussing the  
3 formation process in detail and only mentioned the context on page 3060 line 16-17, that  
4 during the time of maximum ACME formation the PUC is strongest and getting unstable at  
5 the end of the upwelling period.

6 *Could a cap be formed in spring time over a structure that would be cold and fresh at*  
7 *subsurface, with the formation related to subsurface eddying?*

8 - With the formation of an ACME, a subsurface water volume is established within the eddy  
9 core (at around 80-100 m depth) that is largely isolated from the surroundings and transported  
10 westwards with the eddy. The mixed layer above the eddy core is not similarly isolated  
11 because of the weaker eddy rotation near the surface. Water exchange above the eddy core  
12 with the surroundings is thus much more effective. The weaker surface anomaly of ACMEs  
13 compared to cyclones or anticyclones might be maintained by vertical mixing between the  
14 mixed layer and the eddy core resulting in weak cold and fresh mixed layer anomalies.

15 *3.4: eddy structure. Very nice summary statistics. However, on table 3, I am not sure of the*  
16 *consistency of the 5 comparisons. One difference; for 2 to 5; diff of T-anomalies in*  
17 *anticyclone-cyclone=1.2°C, whereas for 1 it is 2.1°C? (also larger diff for salinity in 1: 0.29,*  
18 *compared to 0.15 for 2 to 4). Why is there such a large difference, which seems to have*  
19 *mostly originated from cyclones? Could it be that at the chosen distance from cyclone core,*  
20 *one tends to be into an anticyclonic structure: this would be somewhat surprising, but...?*

21  
22 - To explain the differences between the climatologies we included in table 1 the mean  
23 temperature and salinity values in a small box in TANWA in 100 m depth during June. The  
24 order of the climatologies from warm (saline) to colder (fresher) values is MIMOC, WOA,  
25 CSIRO, Levitus. This explains the highest (lowest) temperature anomaly for cyclones  
26 (anticyclones) using the MIMOC climatology and a decreasing (increasing) anomaly with the  
27 climatologies WOA, CSIRO and Levitus. The same is valid for salinity. In our example box  
28 the MIMOC climatology is nearly 0.5°C warmer and 0.3 more saline than the CSIRO  
29 climatology. These differences between the different climatologies are of the same order of  
30 magnitude than the water mass anomalies in the eddy cores.

31  
32

	Cyclones (CE)		Anticyclones (AE)		Difference (CE-AE)	
	Temp [°C]	Salt	Temp [°C]	Salt	Temp [°C]	Salt
<b>Next Profile Out</b>	-1.22	-0.26	0.87	0.13	-2.09	-0.39
<b>MIMOC</b>	-0.56	-0.32	0.60	-0.17	-1.16	-0.15
<b>WOA</b>	-0.32	-0.10	0.85	0.05	-1.17	-0.15
<b>CSIRO</b>	-0.21	-0.08	0.94	0.06	-1.15	-0.14
<b>Levitus</b>	-0.16		0.97		-1.13	
	Mean temperature (14.5N to 15.5N / 18.5W to 19.5W) at 100m depth, during June			Mean salinity (14.5N to 15.5N / 18.5W to 19.5W) at 100m depth, during June		
	Temp [°C]			Salt		
<b>MIMOC</b>	15.06			35.80		
<b>WOA</b>	14.66			35.64		
<b>CSIRO</b>	14.60			35.52		
<b>Levitus</b>	14.53					

2

3 **Table 1:** Upper table: On the left different mean temperature and salinity anomalies of cyclones and  
4 anticyclones (anticyclones + ACMEs) of the first 350 m relative to reference profile (Next Profile Out) or  
5 different climatologies (CSIRO CARS2009a V1.1 climatology, monthly WOA09 climatology, monthly MIMOC  
6 V2.2 climatology, monthly Levitus94 climatology with salt values not included in monthly base). Right column  
7 shows the difference between mean anomalies of cyclone and anticyclone in each case. Lower Table: Mean  
8 temperature and mean salinity in a box of 14.5N to 15.5N / 18.5W to 19.5W in 100 m depth during June of the  
9 different climatologies.

10

11 The difference between the mean temperature (salinity) anomaly of anticyclones and cyclones  
12 is around 1.15°C (0.15) for all climatologies (see table 1), which one would expect, if all  
13 climatologies behave similarly. The differences derived by using the “next profile outside”  
14 are instead larger when compared to the differences derived by using the climatologies. As  
15 suggested by the reviewer, the “next profile outside” could be located in a neighboring eddy  
16 of reversed polarity. While we used only reference profiles outside of eddies (as identified by  
17 the eddy detection algorithm), we cannot exclude that eddy borders are inaccurately  
18 determined due to noise in the SLA data or the reference profile is located near a neighboring  
19 eddy of reversed polarity. Such a possible influence is discussed in an additional paragraph at  
20 page 3046 line 1:

1  
2 “The differences in the mean anomalies depend on the used reference profiles. Besides the  
3 “next profile outside”, we used different climatologies as reference. However, the differences  
4 between the climatologies are of similar magnitude than the derived mean anomalies of the  
5 different eddy types (Table 1). When using the “next profile outside” as reference we  
6 obtained larger mean anomalies, which could suggest that the “next profile outside” is  
7 systematically biased by nearby eddies of reversed polarity (which are not detected perfectly  
8 by the eddy detecting methods). However, in particular in regions with strong gradients/fronts  
9 (e.g., CVFZ, coastal upwelling) with strong seasonality and variability, the “next profile  
10 outside” should deliver the most realistic background condition surrounding an eddy and thus  
11 should be preferably used to calculate water mass anomalies transported by eddies.”

12  
13 *3.5: when estimating, volumen (mass), assumption of coherency (close streamlines) to 350m.*  
14 *Why this choice? (as one goes down, geostrophic velocity would diminish, thus water would*  
15 *be less trapped).*

16 - We choose 350 m depth as maximal trapping depth as the mean temperature and salinity  
17 anomaly in the eddy vanishes around that depth (see in the submitted manuscript page 9, line  
18 33-34). The reduction of the anomaly with depth is associated with reduced trapping of the  
19 water mass inside the eddy core due to a reduction of the rotational velocity with depth below  
20 the eddy core.

21 *I am slightly flustered by the estimates of transport and release based on ASA and AHA, as*  
22 *they assume implicitly that there is horizontal compensation of mass, thus heat/salt by*  
23 *reference water (thus rather different when one uses reference profile or the climatologies 2*  
24 *to 5). Also, clearly, one expects partial compensation between the cyclones and anticyclones,*  
25 *and thus the net estimate will be very dependent to how structure are identified, how the*  
26 *statistics are established and how they are tracked. I am not convinced that these*  
27 *computations bring any relevant estimate (at least order of magnitude).*

28 - We agree with the reviewer: the assumption behind our calculation of ASA and AHA is the  
29 compensation of mass with background (next profile outside) conditions. In this sense, our  
30 results represent a first order estimate of the heat and salt transports associated with westward  
31 migrating cyclones and anticyclones. These heat and salt transports are, when compared to

1 surface heat and freshwater fluxes, a non-negligible effect in the heat and freshwater budget  
2 of the TANWA, which in our opinion is worth to be noted.

3 *After, bottom page 20 and 21, estimate of transport of SACW yields more robust results with*  
4 *strong differences between structures that are carefully analyzed (better transport by ACME*  
5 *and then cyclones. . .; but for anticyclones, is it compatible with earlier statement on U/C on*  
6 *good water trapping in these structures). An important role of eddies is identified to transport*  
7 *SACW from the coast to the west (and all the way to Cap Verde front?)*

8 - The main reason for the weak water mass anomalies in anticyclones seems to be the  
9 formation mechanism. During boreal summer, which is the dominant formation period,  
10 anticyclones are formed on the warm side of the southward surface boundary current. In this  
11 case, the water mass anomalies in the cores are very weak from the beginning.

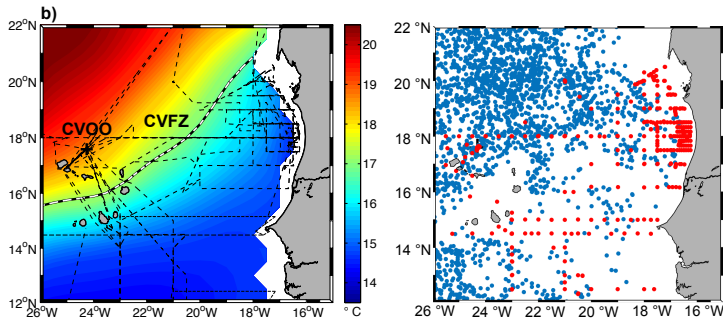
12 To comment on the nonlinearity, i.e. the trapping of water mass anomalies, we shortly discuss  
13 the differences between the different eddy types in the following. After their generation,  
14 eddies of all three types propagate westward with a speed,  $c$ , of about  $3.00 \pm 2.15 \text{ km day}^{-1}$ ,  
15 which is in general agreement with the first baroclinic mode Rossby wave phase speed at that  
16 latitude range. The maximum surface swirl velocity,  $U$ , as obtained from the surface  
17 geostrophic velocity of in SLA detected eddies is on average  $16 \pm 10 \text{ km day}^{-1}$  in cyclones,  $15$   
18  $\pm 10 \text{ km day}^{-1}$  in anticyclones and  $14 \pm 9 \text{ km day}^{-1}$  in ACMEs. This indicates highest  
19 nonlinearity for cyclones  $\alpha = U/c = 5.2$ , followed by anticyclones  $\alpha = 4.9$  and ACMEs  $\alpha = 4.6$ .  
20 Due to this nonlinearity the exchange between eddy interior (eddy core) and surrounding  
21 water is limited and hence they are able to trap and transport water masses. However, the  
22 nonlinearity of ACMEs is much large at the subsurface eddy core and thus the trapping can be  
23 estimated to be most effective in ACMEs. During a recent research cruise of the R/V Meteor  
24 (M 105), for example, an ACME could be crossed in the TANWA. The ADCP zonal and  
25 meridional currents show a baroclinic, anticyclonic rotation flow, with a maximum swirl  
26 velocity of about  $31 \text{ km day}^{-1}$  at about 100 m depth, in that depth  $\alpha = 13$  (see more in  
27 Karstensen et al. 2016).

28

29 *Figures 2 and 3: the tracks on fig.2b of cruises do not always cover the red dot of cruise*  
30 *CTDs in Fig. 3 (for example near 15°N or 13°N).*

31

1 - Thank you very much. We corrected the figure. Unfortunately the cruise tracks in figure 2b  
2 were not complete. We create a new figure including all cruise tracks, the red dots of figure 3  
3 should now be covered by the cruise tracks in the new figure 2b.

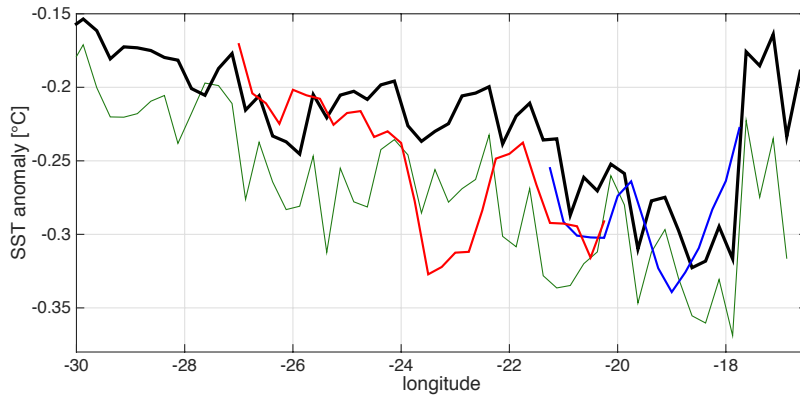


4  
5 **Figure 2:** Mean potential temperature (b) at 100 m depth in the TANWA from the MIMOC  
6 Climatology (Schmidtko et al., 2013). The thick black/white line indicates the CVFZ. The  
7 thin dashed lines mark cruise tracks of 20 research cruises to the TANWA. The right panel  
8 shows a map with the locations of available profiles taken in the TANWA between 1995 and  
9 2013. Red dots mark shipboard CTD stations and blue dots locations of Argo float profiles.

10 *Figure 9, I am wondering how one can separate ACME from other anticyclones for their*  
11 *generation in the source region? (to be more specific: at what point in eddy life is SST used to*  
12 *characterize whether anticyclone is an ACME or not).*

13 - This is an interesting point. We calculated the difference of the SST anomaly in the eddy  
14 core for ACMEs as function of longitude (Figure 3). As questioned by the reviewer, there is  
15 indeed a large variability in the SST anomaly with smaller values near the coast, an abrupt  
16 increase toward offshore at about 18°W and a continuous weakening further offshore during  
17 westward eddy propagation.

1



2

3 **Figure 3:** SST anomaly of the eddy core as function of longitude. Black – mean SST anomaly  
4 of all detected ACMEs from satellite data; Green, red, blue – SST anomaly of 3 different  
5 ACMEs where glider or shipboard observations during the lifetime of the eddies were  
6 conducted and clearly identified the eddy as ACME.

7 We do not include a threshold in eddy life to detect ACMEs and searched for anticyclones  
8 with reduced SST also in the source region. The eddy detection methods could not detect an  
9 eddy near to the coast, as it requires at least structures larger than 80 km on diameter and with  
10 a lifetime of more than a week. Hence, detection signals from the near-coastal  
11 ACME/anticyclone generation region and eddies just generated near to the coast are not  
12 included in the statistics. Therefore we think that ACMEs could not be misleading as  
13 anticyclones (or vice versa) near to the coast. Nevertheless, the development of the SST  
14 anomalies including the sudden increase (likely when the eddy leaving the upwelling area)  
15 followed by a continuous decrease (likely associated with the continuous weakening of the  
16 eddy structure) of the absolute anomaly is very interesting but beyond the scope of this work.

17 *Figure 12: for ACME, left sections and right average profiles are compatible for ACME, but*  
18 *show same anomaly sign for T and S through the vertical profile. It is worth mentioning that*  
19 *there S dominates over T for horizontal density gradients below the eddy core (somehow, I*  
20 *did not see that mentioned in the text; lines 22-23 of 3.4.2 state the opposite, but probably*  
21 *only refer to cyclones and anicyclones). (fully compatible with figure 15)*

22 - We added one sentence in the manuscript at page 3063 line 15. Now, we are also mentioned  
23 that S dominates over T for horizontal density gradients below the eddy core for ACMEs:



1 “Note, that beneath the eddy core (>150 m depth) horizontal density anomalies are dominated  
2 by salinity with temperature playing a minor role.”  
3

1 **Anonymous Referee #2**

2 *This study provides a thorough analysis of the eddy characteristics in the Tropical North*  
3 *Atlantic Ocean, merging various satellite and in-situ datasets. The paper provides a very*  
4 *interesting description of the eddy properties, with a special focus on their vertical structures*  
5 *and associated crossshore transports from the near-coastal upwelling region to the offshore*  
6 *ocean. I really appreciated i) the proposed discrimination between "regular" anticyclones*  
7 *and anticyclonic mode water eddies, ii) the use of satellite sea- surface salinity data which*  
8 *are barely used in studies dealing with mesoscale activity. I really liked reading this paper*  
9 *which is well-written and conveniently organized. The conclusions are supported by the use of*  
10 *appropriate methods and data. I have only some minor comments/suggestions that could*  
11 *probably help to improve the quality and clarity of the paper:*

12 Thank you very much for this evaluation.

13 **Abstract:**

14 *As the number of eddies per year is highly dependent of the minimum lifetime used in the*  
15 *tracking algorithm, I strongly recommend to mention this duration.*

16 - We agree and added the information of the minimum lifetime (7 days) used in the tracking  
17 algorithm to the abstract (page 3044, line 13-15):

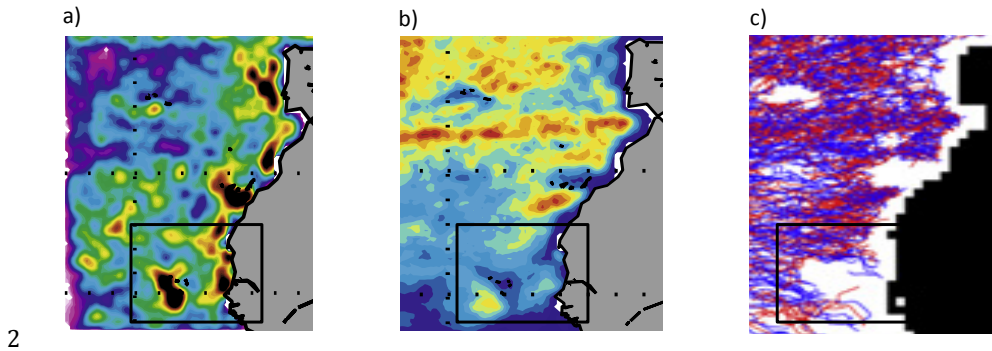
18 “About  $146 \pm 4$  eddies per year with a minimum lifetime of 7 days are identified (52%  
19 cyclones, 39% anticyclones, 9% ACMEs) with rather similar mean radii of about  $56 \pm 12$  km.”

20 **Introduction:**

21 *The introduction is concise and well written. p.3045, L18-21. It is mentioned that previous*  
22 *studies found a low eddy activity in the TANWA region (p.3045, L18-21). However, among*  
23 *the 4 major upwelling system, the TANWA region has been shown to be one of the most active*  
24 *in terms of eddy generation, both at the coast and around the Cap-Vert islands [see for*  
25 *instance Figure 1 in Chaigneau et al., 2009].*

26 - As correctly stated by the reviewer high mesoscale activity in terms of eddy generation is  
27 shown by Chaigneau et al 2009 for the TANWA region with similar hot spots for eddy  
28 generation around Cap-Vert and the Cape Verde Islands as we could identify in our

1 manuscript.



3 **Figure 4:** Extraction of eastern Atlantic from a) Chaigneau et al. 2009 Figure 1 showing the  
4 first detection of eddies, b) Chaigneau et al. 2009 Figure 2 showing the frequency of long-  
5 lived eddies (>35 days) and c) Chelton et al. 2011 Figure 4 showing trajectories of long-lived  
6 eddies (>16 weeks).

7 In the introduction we wanted to point to a difference between former studies and our studies  
8 regarding the occurrence of long-lived eddies. In the former studies (Figure 4 b,c) the number  
9 of long-lived eddies was found to be small or not existing in parts of the TANWA, while in  
10 our study long-lived eddies with coastal waters trapped in their cores could be observed as far  
11 as 800 km offshore at the CVOO mooring. However, we agree with the reviewer that the  
12 sentence was rather strict and not fully correct and rephrased the section in the introduction  
13 (page 3045 , line 18-23) from

14 „However, global as well as regional satellite based studies of eddy distribution and  
15 characterisation (Chelton et al. (2007), Chaigneau et al. (2009), Chelton et al. (2011)) found  
16 eddy activity in the TANWA low and with the absence of long-lived eddies (>112 days  
17 referred to Chelton et al. (2007), >35 days, referred to Chaigneau et al. (2009)).“

18 to

19 „However, global as well as regional satellite based studies of eddy distribution and  
20 characterisation (Chelton et al. (2007), Chaigneau et al. (2009), Chelton et al. (2011)) found  
21 high eddy activity in terms of eddy generation in the TANWA, but only rare occurrence of  
22 long-lived eddies (>112 days referred to Chelton et al. (2007), >35 days, referred to  
23 Chaigneau et al. (2009)).“

1

2 *p. 3047, L11. Please, mention the latitude of Cap Blanc.*

3 - We added the latitude of 21°N of Cap Blanc at page 3047 and line 11 of the manuscript:

4 “During boreal summer the MC re-establishes contemporaneously to the suppression of  
5 coastal upwelling south of Cap Blanc at 21°N (Peña-Izquierdo et al., 2012).

6 *p.3047, L19-20, It is mentioned that one of the topics investigated in the manuscript is the*  
7 *efficiency of mesoscale eddies in dissolving existing gradients. I found this sentence rather*  
8 *unclear and I don't think the authors explicitly study the role of mesoscale eddies on the*  
9 *gradients' distribution. Please explain, rephrase or remove.*

10 - We rephrase the sentence (page 3047 line 19-20) from:

11 „The efficiency of mesoscale eddies within the TANWA in dissolving existing gradients and  
12 transporting cold, less saline and nutrient-rich SACW from their generation regions near the  
13 coast into the open ocean is one topic investigated in this paper.“

14 to

15 “The efficiency of mesoscale eddies to transport cold and less saline SACW from their  
16 generation regions near the coast into the open ocean where NACW dominates is one topic  
17 investigated in this paper.”

18 *Figure 1. I recommend including in the Figure Caption, the nomenclature of the depicted*  
19 *currents.*

20 - We added the nomenclature of the depicted currents in the Figure Caption of Figure 1 (page  
21 3082):

22 “Schematic of the current system of the eastern tropical North Atlantic (red arrows; North  
23 Equatorial Current (NEC), Canary Current (CC), Poleward Under Current (PUC), Mauretania  
24 Current (MC), north Equatorial Counter Current (nNECC), Guinea Current (GC), North  
25 Equatorial Under Current (NEUC)) a) in boreal spring and b) in boreal autumn. Black Arrows  
26 are mean wind vectors, green areas indicate seasonal mean SST<21°C. Blue color represents  
27 topography and the dashed box indicates the TANWA area. The mean position of the

1 Intertropical Convergence Zone (ITCZ) in autumn is indicated by the two black dashed lines  
2 in b).”

### 3 **Data and methods:**

4 *2.1.1. Please, mention which SLA product was used ("two-sat-merged" or "all-sat-merged")*

5 - We added the information that the SLA product “all-sat-merged” is used in the study (page  
6 3048, line 8-10):

7 “The delayed-time reference dataset “all-sat-merged” of SLA (Version 2014), which is used  
8 in the study, is produced by Ssalto/Duacs and distributed by AVISO (Archiving, Validation,  
9 and Interpretation of Satellite Oceanographic), with support from CNES  
10 [<http://www.aviso.altimetry.fr/duac/>].“

11 *2.1.2. The authors used the geometrical approach (GEO) developed by Nencioli et al.*  
12 *(2010). However in this method, the eddy edge is not identified by the longest closed streamline*  
13 *around the eddy center (such as in Chaigneau et al., 2009) but by the closed streamline*  
14 *associated with the strongest swirl velocity. This difference between the longest closed*  
15 *streamline and the Nencioli’s criterion can induce strong differences in the eddy radius*  
16 *distribution (e.g. see Figure 4). Furthermore the Nencioli’s method needs to specify 4*  
17 *constraints for the identification of eddy centers and edges. Thus, I would recommend the*  
18 *authors describe in details this eddy identification method and how they adapt the constraints*  
19 *for the TANWA region.*

20 - That is correct. Unfortunately the GEO-method was only poorly described before. We  
21 rephrase paragraph 2.1.2 to improve the description of the eddy detection algorithms (page  
22 3049-3050).

23 „In order to detect eddy-like structures two different methods are applied to the SLA data.  
24 The first method, the Okubo-Weiß-Method (OW-method; Okubo (1970), Weiss (1991)), has  
25 been frequently used to detect eddies using satellite data as well as the output from numerical  
26 studies (e.g. Isern-Fontanet et al. (2006), Chelton et al. (2007), Sangrà et al. (2009)). The  
27 basic assumption behind the OW-method is that regions, where the relative vorticity  
28 dominates over the strain, i.e. where rotation dominates over deformation, characterize an  
29 eddy. In order to separate strong eddies from the weak background flow field a threshold  
30 needs to be identified. For this study the threshold is set to  $W_0 = -0.2 \cdot \sigma$ , where  $\sigma$  is the

1 spatial standard derivation of the Okubo-Weiß parameter  $W = s_n^2 + s_s^2 - \omega^2$ . Here,  
2  $s_n = \frac{\partial u}{\partial x} - \frac{\partial v}{\partial y}$  is the normal strain,  $s_s = \frac{\partial v}{\partial x} + \frac{\partial u}{\partial y}$  is the shear strain and  $\omega = \frac{\partial v}{\partial x} - \frac{\partial u}{\partial y}$  is the  
3 relative vorticity. A similar definition of the threshold was used in other eddy studies applying  
4 the OW-method (e.g. Chelton et al. (2007)). The maximum (minimum) SLA marks the eddy  
5 center.

6 The second method for eddy detection is based on a geometric approach (GEO-method)  
7 analyzing the streamlines of the SLA derived geostrophic flow. An eddy edge is defined as  
8 the outmost streamline with the strongest swirl velocity around a center of minimum  
9 geostrophic velocity (Nencioli et al., 2010). For the detection of an eddy the algorithm  
10 requires two parameters  $a$  and  $b$  to be defined. The first parameter,  $a$ , is a search radius in grid  
11 points. Inside the search radius, the velocity reversal across the eddy center is identified ( $v$   
12 component on an east-west section,  $u$  component on a north-south section). The second  
13 parameter,  $b$ , is used to identify the point of minimum velocity within a region that extends up  
14 to  $b$  grid points (for a more detailed description of the method see Nencioli et al. (2010)).  
15 After a few sensitivity tests in comparison with the results of the OW-method and following  
16 the instructions of Nencioli et al. (2010), we set  $a=3$  and  $b=2$ . Optimal results were obtained  
17 when we linearly interpolated the AVISO velocity fields onto a 1/6 by 1/6 degree grid before  
18 we applied the algorithm (for more information see also Liu et al. 2011). If an eddy is  
19 detected an eddy center is identified analog to the OW-method as maximum (anticyclone) or  
20 minimum (cyclone) of SLA within the identified eddy structure.”

21 *p. 3050, L.4-11. The eddy tracking algorithm is also unclear. Please rephrase. In particular it*  
22 *is unclear if the authors used a threshold of 7 days (e.g. L.5) or 14 day (L.9) to identify an*  
23 *eddy. How the authors dicreminate between distinct eddies that could have the same polarity*  
24 *in the search radius ? The exact definition of the search radius (10 or 60 km ?) is also*  
25 *unclear. If eddy centers are defined by local extrema in SLA (p. 3050, L-1) how can the*  
26 *authors find another eddy center within 10 km with a grid resolution of 25 km ? Did the*  
27 *authors used eddy centroids instead of local extrema in SLA ?*

28 - The unclear explanation of the tracking algorithm is also noted by referee 1. We rephrased  
29 this paragraph and added additional information in order to improve the structure, which  
30 hopefully help to better understand the applied algorithms (at page 3050 line 3 to 11):

31 “When applying the two different eddy detection methods to the SLA data from the TANWA  
32 region, we used the same eddy detection thresholds for both methods, i.e. a feature only

1 counts as an eddy, if its radius is larger than 45 km and it is detectable for a period of more  
2 than 7 days. Note, as the identified eddy areas are rarely circular we used the circle-equivalent  
3 of the area of the detected features to estimate the radius. For eddy tracking both eddy  
4 detection methods use the same tracking algorithm. An eddy trajectory was calculated if an  
5 eddy with the same polarity was found at least in 7 consecutive SLA maps (corresponding to  
6 one weeks) within a search radius of up to 50 km. Due to e.g. errors in SLA mappings  
7 (insufficient altimetric coverage) an eddy could vanish and reemerge after a while. Therefore  
8 we searched in 14 consecutive SLA maps (corresponding to 2 weeks) in a search radius of up  
9 to 100 km after an eddy disappearance, if eddies with the same polarity reemerges. If more  
10 than one eddy with the same polarity emerge within the search radius, we defined the  
11 following similarity parameter to discriminate between the eddies:

$$13 \quad X = \sqrt{\left(\frac{\text{distance}}{100}\right)^2 + \left(\frac{\Delta \text{radius}}{\text{radius}_0}\right)^2 + \left(\frac{\Delta \text{vorticity}}{\text{vorticity}_0}\right)^2 + \left(\frac{\Delta \text{EKE}}{\text{EKE}_0}\right)^2}, \quad (1)$$

14 which include four terms including the distance and the difference of the two radii, mean  
15 vorticities and mean EKE of the eddies.  $\text{radius}_0$ ,  $\text{vorticity}_0$  and  $\text{EKE}_0$  are the mean radius,  
16 vorticity and EKE of all identified eddies in TANWA. The eddy with the smallest X is  
17 selected to be the same eddy.”

18 *Finally I did not understand when the OW or GEO method is preferred in the results Section.*  
19 *.. please, clarify.*

20 - That is correct. It was not stated in the results section, which algorithm is preferred. Please  
21 note, that the whole analysis was repeated with both algorithms for comparison and all results  
22 were obtained for both algorithms separately. This is now also pointed out in the manuscript  
23 on page 3050 line 10:

24 „To give an idea of the uncertainty related to the detection technique both methods are  
25 applied to the data. Every step is computed separately with both methods and the results are  
26 compared.“

27 However, as mentioned in the manuscript both algorithms show very similar structures and  
28 results for every stated point in the manuscript (only exception is maybe the first detection of  
29 eddies near the coast, where the local maximum in the number of newly detected eddies is  
30 shifted slightly offshore for the GEO-method compared to the OW-method, the structure is  
31 still the same though). So we decided not to show nearly identical figures and only show the

1 results of the OW-method for the main results. In the following we present in detail for which  
2 part of the results the OW or the GEO method or a mean of both is used and where we  
3 inserted additional sentences in the manuscript to clarify that issue:

4 3.1 Eddy statistics from SLA data:

5 Both algorithms are used and listed separately in table 1 of our submitted manuscript.

6

7 3.2 Formation areas and pathways and 3.3 Seasonal variability of eddy generation

8 The results of the OW-method are shown in Figure 7, 8, 9 and Figure 10. We included the  
9 information in the mentioned figure captions:

10

11 “**Figure 7:** Total numbers of eddies generated within  $1^\circ \times 1^\circ$  boxes (colors) based on the  
12 results of the OW-method. Marked are the headlands Cap Timris (Mauretania), Saint-Louis  
13 (Senegal), Cap Vert (Senegal) and the Islands Santo Antão (Cape Verde) and Fogo (Cape  
14 Verde), which can be associated with the most productive eddy generating regions. The thick  
15 solid black line along  $18^\circ\text{W}/19^\circ\text{W}$  separates the coastal region from the offshore region.”

16

17 “**Figure 8:** Number of eddies generated in  $1^\circ \times 1^\circ$  boxes (a, c, e) and total number of eddies  
18 detected in  $1/6^\circ \times 1/6^\circ$  boxes based on the results of the OW-method (b, d, f) for cyclones (a,  
19 b), anticyclones (c, d) and ACMEs (e, f). In b), d) and f) eddies are only counted with a  
20 lifetime larger than 35 days. In b), d), and f) main eddy propagation corridors are indicated by  
21 solid black lines and thick black arrows, main generation spots by circles with crosses. The  
22 thick solid black line along  $18^\circ\text{W}/19^\circ\text{W}$  in a), c) and e) separates the coastal region from the  
23 offshore region.”

24

25 “**Figure 9:** Seasonal cycle of the number of newly detected eddies per year based on the  
26 results of the OW-method in the coastal region as shown in Figures 7 and 8. In a) all eddies  
27 are marked by the black line, cyclones by the blue line and all anticyclonic eddies by the  
28 orange line. In b) anticyclonic eddies are separated into anticyclones (red line) and ACMEs  
29 (green line). The shaded areas around the lines represent the standard error.”

30

31 “**Figure 10:** Phase of the annual harmonic of the number of detected eddies in  $2^\circ \times 2^\circ$  boxes  
32 based on the results of the OW-method for a) cyclones and b) anticyclones. Phases are only  
33 shown for boxes with an amplitude larger than 5 eddies. Phase is given in month of the year  
34 with maximum eddy number.”



1  
2  
3  
4  
5  
6  
7  
8  
9  
10  
11  
12  
13  
14  
15  
16  
17  
18  
19  
20  
21  
22  
23  
24  
25  
26  
27  
28  
29  
30

### 3.4.1 Surface anomalies related to eddies

The eddy centers obtained from the OW-method are used to build the composites of Figure 11. We added the information in the figure caption:

**Figure 11:** Composites of SLA, SST and SSS of a cyclone, anticyclone and ACME in TANWA based on the results of the OW-method. Composite SLA for each eddy type and the associated geostrophic velocity (white arrows) are shown in a), b) and c); SST in d), e) and f); and SSS in g), h) and i), respectively. The solid circles mark the mean eddy radius. ,,

### 3.4.2 Vertical structure of eddies and all following sections regarding the vertical structure

We co-locate, in space and time, vertical profiles with eddy surfaces identified in the SLA data. Both algorithms are required to identify an eddy, so we are using a combination of the OW and the GEO-method for that purpose. However, this procedure is already described on page 3053 line 4-7 of the manuscript in the Data & Methods section.

*Section 2.1.3. 20% of the eddies were classified as ACMEs. How the SST and SSS anomalies were computed? An average within their cores or the value at the eddy center? An average along their trajectory? Please, explain.*

- First, fields of SST and SSS anomalies are computed by excluding large-scale variations from the datasets. The large-scale variations are computed by low-pass filtering (with cutoff wavelength of 15° longitude and 5° latitude) the original SST and SSS datasets. The filtered datasets are subtracted from the original datasets preserving the mesoscale variability (SST and SSS anomalies). Second, a box with an extent of 300 km x 300 km around the eddy center is selected. In order to know whether an eddy is cold or fresh in its core, the average value over the edge of the box is subtracted from the average over the eddy center and its closest neighboring grid points. We added one sentence to page 3051 and line 1 to give that information:

“The information whether an eddy is cold/warm or fresh/saline in the core is obtained by subtracting the average value over the edge of the box from the average value over the eddy center and its closest neighboring grid points.”

1 *The authors decided to use cartesian coordinates to depict the composite maps of eddy*  
2 *properties. However they mix eddies having a wide range of eddy radii. It would probably*  
3 *have been more appropriate to use would a normalized distance.*

4 - That is correct. However, we decided to use unscaled coordinates, because in our relatively  
5 small investigation area the majority of eddies is of similar size. In addition, we only use  
6 eddies with a radius between 45 to 70 km to build the composite maps (80 % of all detected  
7 eddies). We add one sentence at page 3051 line 1-3 to the manuscript to give that  
8 information:

9 “The composite plots are based only on eddies with a radius between 45-70 km and an  
10 absolute SLA difference between the eddy centre and the mean along the edge of the 300 km  
11 x 300 km box used for the composites greater than 2 cm.”

12 *A criterion on the eddy amplitude (2 cm) is also applied to construct these maps. How the*  
13 *composite analysis presented in Section 3 varies with the eddy amplitude?*

14 - In order to build distinct composites of SLA, SST and SSS, we only used eddies with an  
15 amplitude greater than 2 cm in SLA. Such eddies typically exist since a while. The criterion is  
16 particularly important for the composites of SSS. If all eddies were used, the SSS anomaly of  
17 the composit was much weaker and lost its (more or less) circular eddy shape. The SLA and  
18 SST composites are much less affected by the chosen amplitude. We add one sentence at page  
19 3061 line 27 to the manuscript to give that information:

20 “Note, that the SSS composites showed only coherent eddy structures when selecting  
21 energetic eddies (i.e., with a radius between 45-70 km and an absolute SLA anomaly >2 cm).  
22 The SLA and SST composites are much less affected by the restriction with regard to the  
23 eddy amplitude.”

24 *Section 2.2. Why the authors decided to retain only Argo float profiles having data down to*  
25 *1000 m if they only study the upper part (0-350m). I guess considering profiles having data*  
26 *only in the firsts 500 m would have considerably increased the number of available data.*

27 - That is correct. As we only study the first 500 m, we could indeed soften the restriction of  
28 continuous data of Argo floats from 1000 m to 500 m. However, changing the restriction only  
29 provides 8 more profiles. We decided that the additional 8 profiles (outside of an eddy) do not  
30 help to improve the statistics significantly.

1 A Table indicating, for each dataset (Argo, mooring, ship data, etc.), the number of profiles  
 2 within Ces, Aes, ACMEs or outside eddies would have been appreciated. Do Argo floats in  
 3 the TANWA have a preference to be trapped within a particular eddy-type or within larger  
 4 and long-lived eddies as mentioned by Pegliasco et al. [2015]?

5 - The randomly distributed profiles of the Argo floats surfaced preferentially in large (= high  
 6 amplitude of SLA), long-live eddies. This is not observed for the shipboard and mooring data.  
 7 In addition the Argo floats surfaced more often in anticyclones, which could also be seen for  
 8 shipboard CTD data. Interestingly, the mooring in contrast records more cyclones passage the  
 9 mooring position (11 events) than anticyclones (7 events). However, we decided not to  
 10 include this table in the present manuscript as it does not represent, in our opinion, substantial  
 11 additional information.

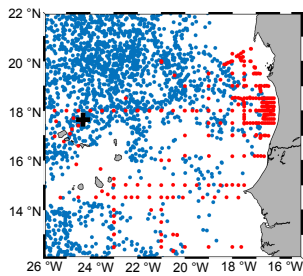
12 **Table 2:** Separation into all different types of data (Argo float, shipboard CTD and CVOO  
 13 mooring) and the associated profiles in Cyclones, Anticyclones and ACMEs.

	Cyclones	Anticyclones	ACMEs	$\Sigma$ of all profiles
Argos floats	215	300	16	582
Shipboard CTD	79	112	23	163
CVOO mooring	11 eddy events (205 profiles)	7 eddy events (168 profiles)	4 eddy events (56 profiles)	429
$\Sigma$ of all profiles	499	580	95	1174

14

15 *Figure 3. The mooring location is unclear.*

16 - We added the location of the CVOO mooring in figure 3.



17

1 **Figure 5:** Locations of available profiles obtained in the TANWA between 1995 and 2013.  
2 Red dots mark shipboard CTD stations, blue dots locations of Argo float profiles and the  
3 black cross the location of the CVOO mooring.

4 *Section 2.3. p. 3053, L.10-15. Do Pegliasco et al. [2015], who also used Argo floats near the*  
5 *TANWA region but a distinct eddy detection algorithm, also found a similar proportion of*  
6 *floats within eddies ?*

7 - Pegliasco et al. [2015] found 62% of all profiles outside of an eddy, 20% within  
8 anticyclones and 18% within cyclones. If we do the statistics with our full dataset (Argo  
9 floats, shipboard CTD and mooring profiles) we found surprisingly similar numbers of 61%  
10 of all profiles outside of an eddy, 22% within anticyclones and 16% within cyclones.  
11 However, the mooring profiles should be excluded from the data set as we only extracted  
12 eddy events here and a random distribution is not granted. Without the mooring profiles (only  
13 using Argo float and shipboard CTD profiles) around ~29% of all profiles were taken per  
14 coincidence inside of an eddy (71 % profiles outside of an eddy, 16 % within anticyclones, 13  
15 % within cyclones). We added that information in one sentence on page 3053 line 13-15:

16 „Excluding the mooring based profiles, from which we only extracted eddy events, around  
17 ~29% of all profiles (Argo float and shipboard CTD profiles) were taken coincidentally inside  
18 of an eddy. This proportion is in the range of earlier results derived by Chaigneau et al.  
19 (2011), who estimate that ~23% of the eastern upwelling regions in the Pacific Ocean are  
20 covered by eddies and Pegliasco et al. (2015), who found 38% of all profiles in the eastern  
21 upwelling areas covered by eddies.”

22 *p. 3053, L.15-20. Several authors (Castelao, 2014 ; Pegliasco et al., 2015) have constructed*  
23 *their anomalies using profiles outside eddies, within +/- 30 days independently of the*  
24 *considered year. It is unclear if in this manuscript the authors used a similar approach. . . if*  
25 *not, using such an approach would probably strongly increased the number of available*  
26 *anomaly profiles. Furthermore the comparison with other climatologies (CARs, WOA,*  
27 *Levitus) presented in the Results Section would be probably more robust. Also, is there any*  
28 *justification to choose criteria of 120km (why not 150 or 200km ?) and +/- 25 days (why not*  
29 *30 days?) for the reference profile.*

30 - We do not look for reference profiles independently of the considered year. The reasoning  
31 behind the chosen criteria (120 km and 25 days) is that we wanted to have the reference

1 profile reasonably close in time and space to the profile inside the eddy to calculate robust  
2 anomalies, especially with regard to the strong fronts and seasonal changes in the TANWA  
3 and, at the same time, to obtain enough reference profiles to derive robust anomalies.  
4 Applying our restrictions we end up with 998 profiles out of the 1174 profiles in eddies with a  
5 reference profile nearby. For 176 profiles we could not find a reference profile. A further  
6 relaxation of the chosen restriction probably does not improve much the obtained anomalies,  
7 while it increase the uncertainties associated with the large spatial and temporal variability in  
8 the TANWA.

9 *p. 3054, L. 3-4. The authors mention that 95 profiles are within ACMES. However from Fig 5,*  
10 *we only see ~20 profiles within ACMES. Please, explain such a difference.*

11 - This is because a large number of individual profiles are taken at the same position.  
12 Especially at the CVOO mooring 56 profiles were taken during 4 ACME events, but it is only  
13 indicated by one single dot, because it is always at the same position.

#### 14 **Results and Discussion**

15 *Section 3.1. Is there any physical reason why the standard deviation on the eddy radius is*  
16 *much higher when the GEO-method is used?*

17 - We examined the radii identified from the GEO-method in more detail and figured out that  
18 the GEO-method seem to identify sporadic some very large eddies. For example identified the  
19 GEO-method 192 eddies (106 cyclones, 86 anticyclones) with a radius larger than 100 km,  
20 whereas the OW-method detected not one single eddy of that size. It seems that the GEO-  
21 method tends to identify a certain feature as on single eddy rather than dividing it and on the  
22 other hand, the OW-method rather divide one large eddy structure into several smaller eddies  
23 if the OW parameters in some parts of the large eddy does not match the threshold. We  
24 included an additional sentence in the text at page 3057 line 1:

25

26 “The difference in the standard deviation of the eddy radius derived from GEO and the OW-  
27 method is partly due to the identification of few very large eddies using the GEO-method,  
28 which is not the case for the OW-method.”

29

1 *p.3057, L.10 : Is the maximum lifetime constrained by the longitudinal extent of the study*  
2 *area? (e.g. Do anticyclones disappear/dissipate after 280 days or they are no more detected*  
3 *due to the presence of the western boundary at 28W ?)*

4 - Yes, the eddy trajectories are cut off at the western boundary at 28°W (also at the northern  
5 and southern boundaries) and hence the length of the trajectories and therefore also the  
6 lifetime of eddies is restricted to the size of the domain. We applied the eddy algorithms to an  
7 area extending the TANWA region by 4° (to the west, north and south) to avoid spurious  
8 effects of the detection algorithms at the borders. However, we checked the eddy trajectories  
9 and around 12% of all detected eddies in TANWA crossed a border of the domain. The  
10 majority of the eddies leaving the domain are not old and most of them are generated near the  
11 Cap Verde Islands propagating to the west. Nevertheless, some older eddies generated in the  
12 upwelling area are also among them (see for example the longest trajectories of the eddies  
13 represented in figure 1). Therefore, we agree with the reviewer that the mean eddy lifetime is  
14 restricted/biased/underestimated in the paper. In addition to that the eddy tracking algorithms  
15 tend to underestimate the eddy lifetime in general (errors in the eddy tracking/wrong  
16 identification) and hence the significance of the mean eddy lifetime is questionable anyway.  
17 Interestingly, the mean eddy lifetime is consistent for both methods with anticyclones living  
18 longer than cyclones in both methods. We added one sentence to the manuscript on page 3058  
19 line 8 to mention that issue:

20 “In addition the mean eddy lifetime of eddies in TANWA is underestimated due to restriction  
21 of eddy trajectories at the northern, southern and western boundaries.”

22 *p.3057, L.19-20. The dominance of anticyclones is interesting and was also observed in the*  
23 *polarity map of Chaigneau et al. [2009]. Is there any explanation for such a dominance of*  
24 *long-lived anticyclones?*

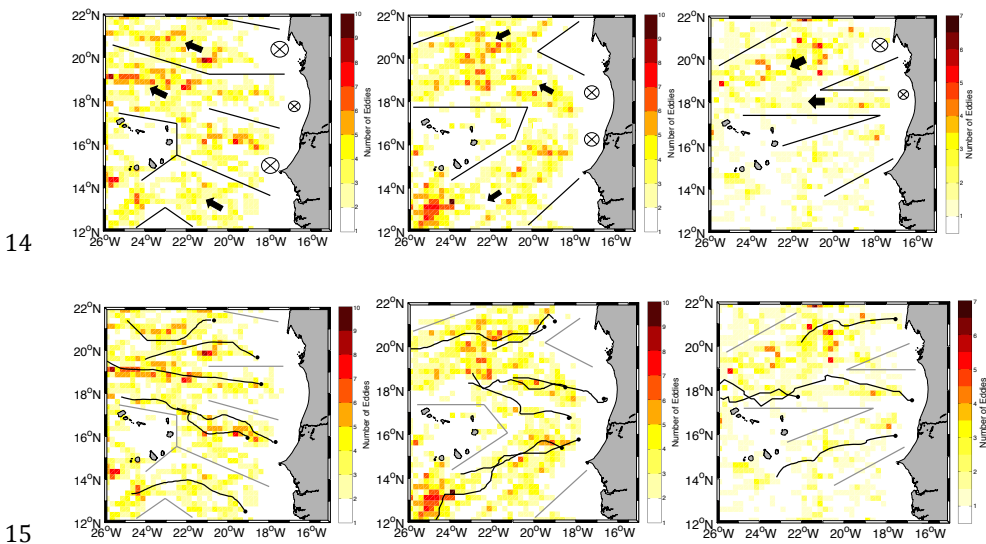
25 - As mentioned correctly by the reviewer the dominance of observed long-lived anticyclones  
26 is also stated by e.g. Chaigneau et al. (2009) or Chelton et al. (2011). In general, the  
27 observational studies show that anticyclones exhibit larger radii, higher SLA amplitudes and  
28 live longer than cyclones. Cushman-Roisin and Tang (1989) demonstrated theoretically that  
29 anticyclonic eddies are generally more robust and merge more freely than cyclones.  
30 Following Cushman-Roisin and Tang (1989), cyclonic eddies are better capable of self-  
31 destruction. They even showed that interactions with surrounding eddies and turbulence are  
32 not necessary to account for the absence of cyclonic eddies in the statistical equilibrium.

1 We decided to added additional information about long-lived anticyclones to the manuscript  
2 (page 3057, line 20):

3 „The dominance of long-lived anticyclones is also shown in the observational studies of  
4 Chaigneau et al. (2009), Chelton et al. (2011) and theoretically proven by Cushman-Roisin  
5 and Tang (1989). The latter authors showed that in an eddying environment anticyclonic  
6 eddies are generally more robust and merge more freely than cyclones producing long-lived  
7 eddies, while cyclones show a higher tendency to self-destruction.“

8 *Section 3.2. A visualization of the eddy trajectories in Figure 8 would be better than a rather  
9 simple schematics of the eddy propagation patterns. Or both of them (schematics and "true"  
10 trajectories) should be presented.*

11 - Referee #1 also noted the rather schematic presentation of the eddy propagation in figure 8.  
12 We decided to follow the suggestion of the reviewer and add trajectories of long-lived eddies  
13 exemplarily showing the eddy propagation direction and pathways (see figure 1).



16 **Figure 6:** Upper row old pictures: Total number of eddies detected in  $1/6^\circ \times 1/6^\circ$  boxes for  
17 cyclones, anticyclones and ACMEs. Only eddies are counted with a lifetime larger than 35  
18 days. Main eddy propagation corridors are indicated by solid black lines and thick black  
19 arrows, main generation spots by circles with crosses. Lower row new pictures: Total number  
20 of eddies detected in  $1/6^\circ \times 1/6^\circ$  boxes for cyclones, anticyclones and ACMEs. Only eddies

1 are counted with a lifetime larger than 35 days. Main eddy propagation corridors are indicated  
2 by solid grey lines and selected trajectories of long-lived eddies. The dots mark the starting  
3 point of the eddy trajectories.

4 *Section 3.4.2. It is unclear why a deepening of the isopycnal below ~120-150m in the ACMEs*  
5 *does not produce a positive temperature anomaly since it should inject warmer water in*  
6 *deeper levels. Please, explain.*

7 - This could only be explained due to the strong SACW anomaly (cold and fresh) within the  
8 eddy core. The water injected into a deeper level due to the deepening of the isopycnals is not  
9 significantly warmer than the surrounding water at that depth. We add one sentence in the  
10 manuscript to explain that issue (page 3063, line 11):

11 “Note, that the cold and fresh SACW in the ACME core does not produce a positive  
12 temperature anomaly when it reaches deeper levels due to the downward bending of isopycnal  
13 surfaces below the eddy core.”

14 *Also, the mean distribution of isotherms and isohaline levels in Figure 12 a-b would have*  
15 *been probably more relevant than isopycnals. A description and quantification of the vertical*  
16 *displacement of the isopycnal layers with depth would have been appreciated.*

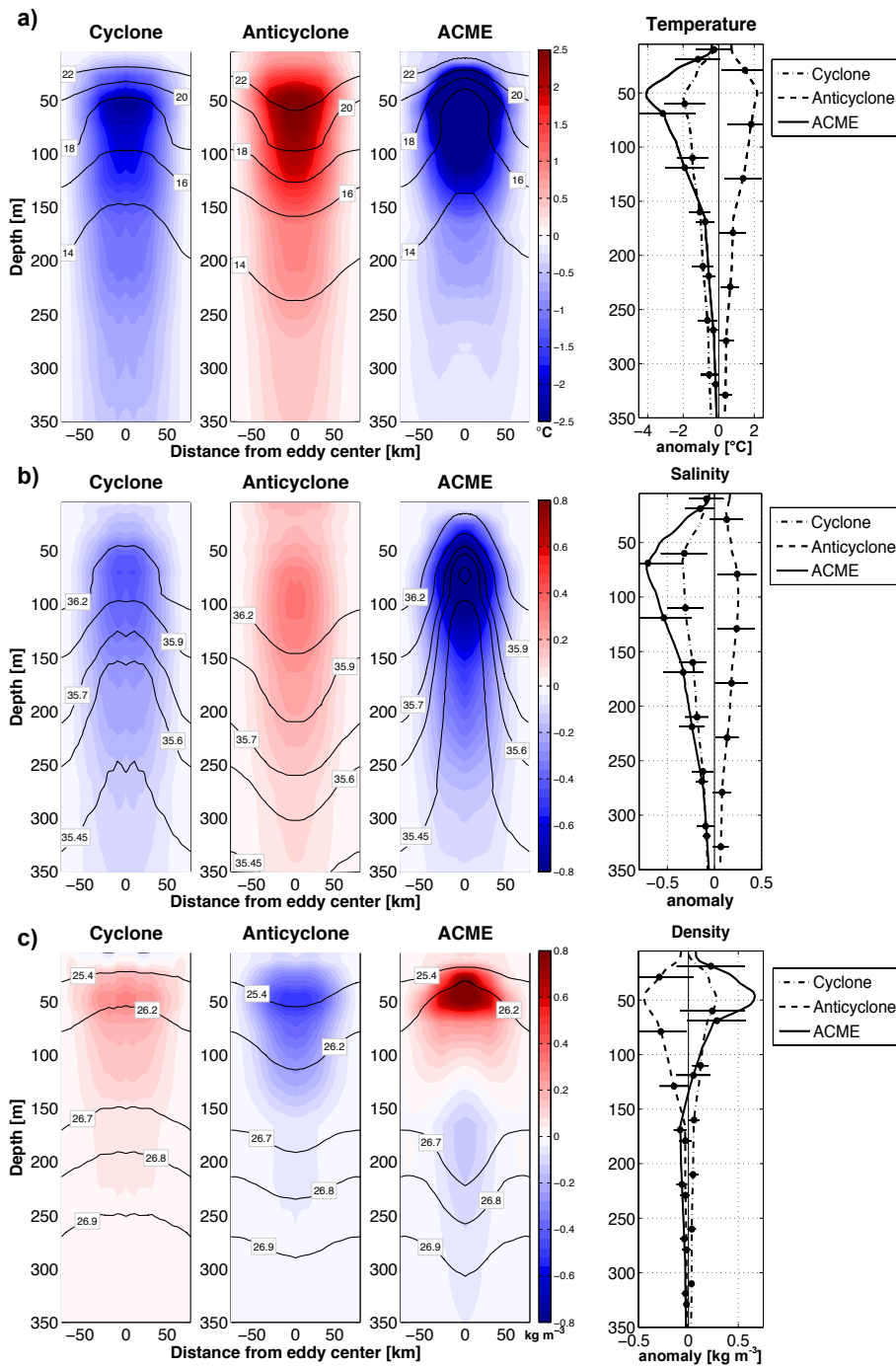
17 - We followed the suggestions of the reviewer and added isotherms and isohaline levels in  
18 Figure 12 a-b and briefly describe the vertical displacement of the isopycnal layers of  
19 cyclones and anticyclones in the manuscript on page 3062 line 25:

20 “This is illustrated by the elevation (deepening) of 25 m (36 m) of the density surface of 26.2  
21  $\text{kg m}^{-3}$  in the core of the cyclone (anticyclone) compared to the surroundings.”

22 For ACMEs at page 3063 line 1:

23 “The mode-water in the core of the ACME exhibits only small density gradients. This is  
24 illustrated by the elevation of 48 m of the density surface of  $26.2 \text{ kg m}^{-3}$  slightly above the  
25 core and the deepening of 52 m of the density surface of  $26.7 \text{ kg m}^{-3}$  beneath the core  
26 compared to the surroundings.”





1

2 **Figure 7:** Vertical structure of the composite cyclone, anticyclone and ACME in TANWA

1 presented as sections across the eddies (left three columns) and mean profiles (right column).  
2 In **(a)** potential temperature, in **(b)** salinity and in **(c)** potential density anomaly relative to the  
3 nearest profile outside of the eddy is shown. Black contour lines in the left three columns  
4 mark mean isotherms, isohalines and isopycnal surfaces. In the right column, solid lines  
5 represent the composite ACME, dashed lines the anticyclone and dashed-dot lines the  
6 cyclone; the error bars at the black dots represent the standard deviation calculated from the  
7 individual anomaly profiles

8 *Section 3.5.1. Figure 14b. It is unclear how ESHF were computed. Please, provide more*  
9 *details since I could not reproduce the obtained HF values.*

10 - The equivalent surface heat flux (ESHF) is computed by using the heat transport of the  
11 eddies (table 4 of the submitted manuscript) times the amount of eddies dissolving during a  
12 year in Area II (see Figure 14a of the submitted manuscript) divided by the surface area of  
13 Area II resulting in a mean heat release in  $\text{W m}^{-2}$ . At the end the ESHF is compared to the net  
14 atmospheric heat flux in Area II derived from the NOC Surface Flux Dataset (Berry and Kent,  
15 2011). We add that information in the manuscript at page 3055 line 24-25:

16 “By multiplying the heat transport of the composite eddies with the amount of eddies  
17 dissolving during a year in a given area (corresponding to an flux divergence) a mean heat  
18 release (in  $\text{W m}^{-2}$ ) and a mean salt release (in  $\text{kg m}^{-2}$ ) was calculated. The mean heat release  
19 can be compared to the net atmospheric heat flux in the area here derived from the NOC  
20 Surface Flux Dataset (Berry and Kent, 2011).”

21 *Section 3.5.2. It is considered in this Section there are only 2 Water Masses between the*  
22 *surface and 350m depth (SACW and NACW). However this region can also be influenced by*  
23 *tropical surface water (at least in the southern part of the TANWA) in the surface layer (0-*  
24 *50m) [e.g. Stramma et al., 2005]. Should the TSW be considered in the WM analysis?*

25 - Tropical surface water (TSW) might only affect the very shallow part of the eddy, the main  
26 body of the eddy is well-separated from the upper ocean with only weak vertical mixing.

27 *It is mentioned (p.3067, L.29) that anticyclones have the same SACW signature as the*  
28 *background. In this case, which Water Mass anticyclones transport and which water mass*  
29 *explain the strong positive T/S anomalies inside their cores?*

1 - If we calculated the water mass anomalies on density surfaces anticyclones transport nearly  
2 no water mass anomaly in their cores. The T/S anomalies in the core (figure 12 – calculated  
3 on depth layers) are only generated by the vertical displacement of isopycnals.

4

#### 5 **References:**

6 Berry, D. I. and Kent, E. C.: Air–Sea fluxes from ICOADS: the construction of a new gridded  
7 dataset with uncertainty estimates, *International Journal of Climatology*, 31, 987-1001, 2011.

8 Chaigneau, A., Eldin, G., and Dewitte, B.: Eddy activity in the four major upwelling systems  
9 from satellite altimetry (1992–2007), *Progress in Oceanography*, 83, 117-123, 2009.

10 Chelton, D. B., Schlax, M. G., and Samelson, R. M.: Global observations of nonlinear  
11 mesoscale eddies, *Progress in Oceanography*, 91, 167-216, 2011.

12 Chelton, D. B., Schlax, M. G., Samelson, R. M., and de Szoeke, R. A.: Global observations of  
13 large oceanic eddies, *Geophysical Research Letters*, 34, L15606,  
14 doi:10.1029/2007GL030812, 2007.

15

16 Cushman Roisin B. and Tang B., 2010: Geostrophic Turbulence and Emergence of Eddies  
17 beyond the Radius of Deformation, *Journal of Physical Oceanography*, 20, 97–113, doi:  
18 10.1175/15200485(1990)020<0097:GTAEOE>2.0.CO;2.

19

20 D’Asaro, E. A.: Generation of submesoscale vortices: A ne mechanism, *Journal of*  
21 *Geophysical Researh*,doi: 10.1029/JC093iC06p06685 93, 6685-6693, 1988.

22 Karstensen, J., Schütte, F., Pietri, A., Krahnmann, G., Fiedler, B., Grundle, D., Hauss, H.,  
23 Körtzinger, A., Löscher, C. R., Testor, P., Vieira, N., and Visbeck, M.: Upwelling and  
24 isolation in oxygen- depleted anticyclonic modewater eddies and implications for nitrate  
25 cycling, *Biogeosciences Discuss.*, doi:10.5194/bg-2016-34, in review, 2016.

26 Liu Y., Changming Dong, Yuping Guan, Dake Chen, James McWilliams, Francesco  
27 Nencioli, Eddy analysis in the subtropical zonal band of the North Pacific Ocean, *Deep Sea*  
28 *Research Part I: Oceanographic Research Papers*, Volume 68, October 2012, Pages 54-67,  
29 ISSN 0967-0637, <http://dx.doi.org/10.1016/j.dsr.2012.06.001>.

30

31 Nencioli, F., Dong, C., Dickey, T., Washburn, L., and McWilliams, J. C.: A Vector  
32 Geometry–Based Eddy Detection Algorithm and Its Application to a High-Resolution  
33 Numerical Model Product and High-Frequency Radar Surface Velocities in the Southern  
34 California Bight, *J Atmos Ocean Tech*, 27, 564-579, 2010.

35 Schütte, F., Karstensen, J., Krahnmann, G., Hauss, H., Fiedler, B., Brandt, P., Visbeck, M., and  
36 Körtzinger, A.: Characteriza- tion of “dead-zone” eddies in the tropical Northeast Atlantic  
37 Ocean, *Biogeosciences Discuss.*, doi:10.5194/bg-2016-33, in review, 2016.

38 Stramma L.,S. Hüttl, J. Schafstall, 2005: Water masses and currents in the upper tropical  
39 northeast Atlantic off northwest Africa, *Journal of Geophysical Research*,110, 2156-2202,  
40 Doi: <http://dx.doi.org/10.1029/2005JC002939>

# 1 Occurrence and characteristics of 2 mesoscale eddies in the tropical 3 northeast Atlantic Ocean

4 F. Schütte <sup>1</sup>, P. Brandt <sup>1,2</sup> and J. Karstensen <sup>1</sup>

5 [1] GEOMAR Helmholtz Centre for Ocean Research Kiel, Kiel, Germany

6 [2] Christian-Albrechts-Universität zu Kiel, Kiel, Germany

7 Correspondence to: F. Schütte (fschuette@geomar.de)

## 8 Abstract

9 Coherent mesoscale features (referred to here as eddies) in the tropical northeast Atlantic  
10 (between 12°N - 22°N and 15°W - 26°W) are examined and characterised. The eddies'  
11 surface signatures are investigated using 19 years of satellite derived sea level anomaly (SLA)  
12 data. Two automated detection methods are applied, the geometrical method based on closed  
13 streamlines around eddy cores, and the Okubo-Weiß method based on the relation between  
14 vorticity and strain. Both methods give similar results. Mean eddy surface signatures of SLA,  
15 sea surface temperature (SST) and salinity (SSS) anomalies are obtained from composites of  
16 all snapshots around identified eddy cores. Anticyclones/cyclones are identified by an  
17 elevation/depression of SLA and enhanced/reduced SST and SSS in its cores. However, about  
18 20% of all anticyclonically rotating eddies show reduced SST and reduced SSS instead. These  
19 kind of eddies are classified as anticyclonic mode-water eddies (ACMEs). About  $146 \pm 4$   
20 eddies per year with a minimum lifetime of 7 days are identified (52% cyclones, 39%  
21 anticyclones, 9% ACMEs) with rather similar mean radii of about  $56 \pm 12$  km. Based on  
22 concurrent in-situ temperature and salinity profiles (from Argo float, shipboard and mooring  
23 data) taken inside of eddies, distinct mean vertical structures of the three eddy types are  
24 determined. Most eddies are generated preferentially in boreal summer and along the West  
25 African coast at three distinct coastal headland regions and carry South Atlantic Central  
26 Water supplied by the northward flow within the Mauretania coastal current system.  
27 Westward eddy propagation (on average about  $3.00 \pm 2.15$  km d<sup>-1</sup>) is confined to distinct  
28 zonal corridors with a small meridional deflection dependent on the eddy type (anticyclones –  
29 equatorward, cyclones – poleward, ACMEs – no deflection). Heat and salt flux out of the

- Florian Schütte 22.4.16 11:17  
**Gelöscht:** associated with
- Florian Schütte 22.4.16 11:18  
**Gelöscht:** patterns
- Florian Schütte 22.4.16 11:18  
**Gelöscht:** detected
- Florian Schütte 22.4.16 11:18  
**Gelöscht:** es
- Florian Schütte 22.4.16 11:20  
**Gelöscht:** data
- Florian Schütte 22.4.16 11:20  
**Gelöscht:** the three eddy types
- Florian Schütte 22.4.16 11:20  
**Gelöscht:** their
- Florian Schütte 22.4.16 11:21  
**Gelöscht:** differences in
- Florian Schütte 22.4.16 11:21  
**Gelöscht:** is
- Florian Schütte 22.4.16 11:21  
**Gelöscht:**
- Florian Schütte 22.4.16 11:22  
**Gelöscht:** that originates from the
- Florian Schütte 22.4.16 11:22  
**Gelöscht:** transport

- 1 coastal region and across the Cap Verde Frontal Zone, which separates the shadow zone from
- 2 | the ventilated [subtropical](#) gyre, are calculated.

## 1 Introduction

2 The generation of eddies in coastal upwelling regions is strongly related to the eastern  
3 boundary circulation and its seasonal variations. Within the tropical Atlantic Ocean off  
4 northwest Africa (TANWA; 12°N to 22°N and 26°W to 15°W), the large-scale surface  
5 circulation responds to the seasonal variability of the trade winds and the north/south  
6 migration of the Intertropical Convergence Zone (ITCZ) (e.g. Stramma and Isemer (1988),  
7 Siedler et al. (1992), Stramma and Schott (1999)). The seasonal wind pattern results in a  
8 strong seasonality of the flow field along the northwest African coast and in coastal upwelling  
9 of different intensity. The coastal upwelling in the TANWA is mainly supplied by water  
10 masses of South Atlantic origin (Jones and Folkard (1970), Hughes and Burton (1974),  
11 Wooster et al. (1976), Mittelstaedt (1991), Ould-Dedah et al. (1999), Pastor et al. (2008),  
12 Glessmer et al. (2009), Peña - Izquierdo et al. (2015)), which are relatively cold and fresh  
13 compared to the North Atlantic waters further offshore. The water mass transition region  
14 coincides with the eastern boundary shadow zone, where diffusive transport pathways  
15 dominate (Luyten et al., 1983) with weak zonal current bands superimposed (Brandt et al.,  
16 2015). The oceanic circulation in the TANWA is most of the time weak and the velocity field  
17 is dominated by cyclonic and anticyclonic eddies. However, global as well as regional  
18 satellite based studies of eddy distribution and characterisation (Chelton et al. (2007),  
19 Chaigneau et al. (2009), Chelton et al. (2011)) found high eddy activity in terms of eddy  
20 generation in the TANWA, but only rare occurrence of long-lived eddies (>112 days referred  
21 to Chelton et al. (2007), >35 days, referred to Chaigneau et al. (2009)). Karstensen et al.  
22 (2015) studied individual energetic eddy events based on a combination of in-situ and satellite  
23 based Sea Level Anomaly (SLA) data, and reported eddy life times of more than 200 days in  
24 the TANWA region. These individual eddies carried water mass characteristics typical for the  
25 shelf region up to 900 km off the African coast. One possible generation area for such eddies  
26 is the Cap-Vert headland at about 14.7°N near the Senegalese coast (Karstensen et al., 2015).  
27 Analysing surface drifter data and high-resolution satellite data, Alpers et al. (2013) described  
28 the evolution of an energetic sub-mesoscale eddy at the Cap-Vert headland that was  
29 presumably generated by flow separation of a wind-forced coastal jet. Earlier studies reported  
30 on the importance of eddy transport in the TANWA region (e.g. Hagen (1985); Barton  
31 (1987); Zenk et al. (1991)). However, characteristics of the eddy field in the TANWA region  
32 such as seasonality in eddy generation, eddy lifetime, vertical structure, or frequency of  
33 occurrence are so far undocumented.

Florian Schütte 22.4.16 11:27

**Gelöscht:** and their recirculation

Florian Schütte 4.4.16 15:42

**Gelöscht:** low and

Florian Schütte 11.4.16 14:57

**Gelöscht:** with the absence

Florian Schütte 12.4.16 12:04

**Gelöscht:** formation

Florian Schütte 22.4.16 11:28

**Gelöscht:**

1 More comprehensive information on eddy dynamics was gained for the Pacific Ocean eastern  
2 boundary upwelling systems. The eddy generation in the northeast Pacific Ocean, off  
3 California and Mexico including the California Current System was studied with high-  
4 resolution models applied to reproduce observed characteristics of the eddy field (Liang et al.  
5 (2012), Chang et al. (2012)). These studies highlight hotspots of eddy generation associated  
6 with local wind fluctuations (e.g. over the Gulf of Tehuantepec and Papagayo), but also  
7 suggest an important role of low-frequency wind and boundary forcing. For the southeast  
8 Pacific Ocean, off Peru and Chile, including the Peru-Chile Current System, Chaigneau et al.  
9 (2008) and Chaigneau et al. (2011) analysed the seasonal to interannual variability of eddy  
10 occurrence as well as the mean vertical structure of eddies based on Argo floats.

Florian Schütte 12.4.16 12:04

Gelöscht: formation

11 A schematic of the current system of the TANWA in boreal spring and in boreal autumn is  
12 presented in Figure 1. In the north of the TANWA the Canary Current (CC) transports cold  
13 water southwards along the African shelf. It detaches from the coast around Cap Blanc (more  
14 specifically at about 20°N during spring and 25°N during autumn) and joins the North  
15 Equatorial Current (NEC) (Mittelstaedt (1983), Mittelstaedt (1991)). The dominant feature  
16 south of the TANWA is the eastward flowing North Equatorial Countercurrent (NECC)  
17 extending over a latitudinal range from 3°N to about 10°N. It has a pronounced seasonal cycle  
18 with maximum strength in boreal summer and autumn, when the ITCZ reaches its  
19 northernmost position. During that period the NECC is a continuous zonal flow across the  
20 entire tropical Atlantic (e.g. Garzoli and Katz (1983), Richardson and Reverdin (1987),  
21 Stramma and Siedler (1988), Polonsky and Artamonov (1997)). When approaching the  
22 African coast, the current is partly deflected to the north feeding a sluggish northward flow  
23 along the coast. This current is referred to as Mauretania Current (MC) and reaches latitudes  
24 up to 20°N (Mittelstaedt, 1991). The strength of the MC is strongly related to the seasonally  
25 varying NECC with a time lag of one month (Lázaro et al., 2005). During boreal winter and  
26 spring when the NECC is pushed to the equator and becomes unstable, the MC becomes weak  
27 and unsteady and only reaches latitudes south of Cap Vert (Mittelstaedt (1991), Lázaro et al.  
28 (2005)). During this period the wind induced coastal upwelling is at its maximum.  
29 Simultaneously, the large-scale pressure gradient set by the southward winds induces an  
30 along-slope subsurface current, known as Poleward Undercurrent (PUC) (Barton, 1989).  
31 During boreal summer the MC re-establishes contemporaneously to the suppression of coastal  
32 upwelling south of Cap Blanc at 21°N (Peña-Izquierdo et al., 2012).

Florian Schütte 22.4.16 11:29

Gelöscht: (

Florian Schütte 22.4.16 11:29

Gelöscht: )

Florian Schütte 22.4.16 11:30

Gelöscht: C

Florian Schütte 22.4.16 11:31

Gelöscht: al current

Florian Schütte 22.4.16 11:31

Gelöscht: p

Florian Schütte 22.4.16 11:31

Gelöscht: u

33 The eastern boundary upwelling is supplied by waters of South Atlantic origin through a  
34 pathway consisting of the North Brazil Current (NBC), the North Equatorial Undercurrent

1 (NEUC) and the PUC. Hence, the purest South Atlantic Central Water (SACW) within the  
2 TANWA is found close to the coast (Figure 2), while further offshore a transition towards the  
3 more saline and warmer North Atlantic Central Water (NACW) is observed. The boundary  
4 between the regimes is associated with the Cape Verde Frontal Zone (CVFZ, Figure 2),  
5 characterized by a sharp horizontal salinity gradient of 0.9 per 10km (Zenk et al., 1991). The  
6 efficiency of mesoscale eddies to transport cold and less saline SACW from their generation  
7 regions near the coast into the open ocean where NACW dominates is one topic investigated  
8 in this paper. In particular, the characteristics of these eddies (size, structure, frequency) and  
9 their potential role in the transport of heat and salt will be examined in more detail.

10 The paper is organized as follows: In section 2, the different data types (satellite derived and  
11 in-situ) will be introduced as well as the techniques to automatically detect and track eddies  
12 from satellite data and to derive their vertical structure. In section 3 the eddy characteristics  
13 (origin, pathways, surface signature) and statistics (frequency) are discussed and the temporal  
14 and spatial variability of eddy generation and eddy pathways are examined. The mean  
15 horizontal and vertical eddy structures are derived and, in combination with the eddy  
16 statistics, used to estimate the transport of volume, heat and salt from the shelf region into the  
17 open ocean. Finally our results are summarized in section 4.

## 18 2 Data and Methods

### 19 2.1 Satellite data

#### 20 2.1.1 SLA, SST and SSS

21 The delayed-time reference dataset “all-sat-merged” of SLA (Version 2014), which is used in  
22 the study, is produced by Ssalto/Duacs and distributed by AVISO (Archiving, Validation, and  
23 Interpretation of Satellite Oceanographic), with support from CNES  
24 [<http://www.aviso.altimetry.fr/duac/>]. The data is a multi-mission product, mapped on a  $1/4^\circ$   
25  $\times 1/4^\circ$  Cartesian grid and has a daily temporal resolution. The anomalies are computed with  
26 respect to a twenty-year mean. Data for the period January 1995 to December 2013 are  
27 considered here. Geostrophic velocity anomalies derived from the SLA provided by AVISO  
28 for the same timespan are also used in this study. Given the interpolation technique applied to  
29 the along track SLA data Gaussian shaped eddies with a radius  $> \sim 45$  km can be detected,  
30 eddies of smaller diameter may be detected but their energy is damped (Fu and Ferrari, 2008).

31

Florian Schütte 1.4.16 14:50

**Gelöscht:** within the TANWA in dissolving existing gradients and

Florian Schütte 1.4.16 14:51

**Gelöscht:** ing

Florian Schütte 11.4.16 14:58

**Gelöscht:** ,

Florian Schütte 11.4.16 14:58

**Gelöscht:** and nutrient-rich

Florian Schütte 22.4.16 11:32

**Gelöscht:** only

Florian Schütte 22.4.16 11:33

**Gelöscht:** ,

Florian Schütte 22.4.16 11:33

**Gelöscht:** while



1 For SST the dataset “Microwave Optimally interpolated Sea Surface Temperature” from  
2 Remote Sensing Systems (www.remss.com) is used. It is derived from satellite microwave  
3 radiometers, which have the capability to measure through clouds. It has a 25 km resolution  
4 and contains the SST measurements from all operational radiometers for a given day. All OI  
5 SST values are corrected using a diurnal model to create a foundation SST that represents a  
6 12-noon temperature [www.remss.com]. Daily data from the outset January 1, 1998 to  
7 December 31, 2013 is used here and mapped similar to the SLA data on a  $1/4^\circ \times 1/4^\circ$   
8 Cartesian grid.

9  
10 Our study also includes sea surface salinity (SSS) data. We make use of the LOCEAN\_v2013  
11 SSS product available from January 1, 2010 until the end of our analysis period (December  
12 31, 2013). The data is distributed by the Ocean Salinity Expertise Center (CECOS) of the  
13 CNES-IFREMER Centre Aval de Traitement des Donnees SMOS (CATDS), at IFREMER,  
14 Plouzane (France). The data is created using the weight averaging method described in Yin et  
15 al. (2012) and the flag sorting described in Boutin et al. (2013). Finally the data is mapped on  
16 a  $1/4^\circ \times 1/4^\circ$  Cartesian grid and consist of 10-day composites.

17

### 18 **2.1.2 Eddy identification and tracking from satellite data**

19 In order to detect eddy-like structures two different methods are applied to the SLA data. The  
20 first method, the Okubo-Weiß-Method (OW-method; Okubo (1970), Weiss (1991)), has been  
21 frequently used to detect eddies using satellite data as well as the output from numerical  
22 studies (e.g. Isern-Fontanet et al. (2006), Chelton et al. (2007), Sangrà et al. (2009)). The  
23 basic assumption behind the OW-method is that regions, where the relative vorticity  
24 dominates over the strain, i.e. where rotation dominates over deformation, characterize an  
25 eddy. In order to separate strong eddies from the weak background flow field a threshold  
26 needs to be identified. For this study the threshold is set to  $W_0 = -0.2 \cdot \sigma$ , where  $\sigma$  is the  
27 spatial standard derivation of the Okubo-Weiß parameter  $W = s_n^2 + s_s^2 - \omega^2$ . Here,  
28  $s_n = \frac{\partial u}{\partial x} - \frac{\partial v}{\partial y}$  is the normal strain,  $s_s = \frac{\partial v}{\partial x} + \frac{\partial u}{\partial y}$  is the shear strain and  $\omega = \frac{\partial v}{\partial x} - \frac{\partial u}{\partial y}$  is the  
29 relative vorticity. A similar definition of the threshold was used in other eddy studies applying  
30 the OW-method (e.g. Chelton et al. (2007)). The maximum (minimum) SLA marks the eddy  
31 center.

32 The second method for eddy detection is based on a geometric approach (GEO-method)  
33 analyzing the streamlines of the SLA derived geostrophic flow. An eddy edge is defined as  
34 the outmost streamline with the strongest swirl velocity around a center of minimum

Florian Schütte 22.4.16 11:36

**Kommentar [1]:** Entweder outmost closed streamline oder strongest swirl velocity...

geostrophic velocity (Nencioli et al., 2010). For the detection of an eddy the algorithm requires two parameters  $a$  and  $b$  to be defined. The first parameter,  $a$ , is a search radius in grid points. Inside the search radius, the velocity reversal across the eddy center is identified ( $v$  component on an east-west section,  $u$  component on a north-south section). The second parameter,  $b$ , is used to identify the point of minimum velocity within a region that extends up to  $b$  grid points (for a more detailed description of the method see Nencioli et al. (2010)). After a few sensitivity tests in comparison with the results of the OW-method and following the instructions of Nencioli et al. (2010), we set  $a=3$  and  $b=2$ . Optimal results were obtained when we linearly interpolated the AVISO velocity fields onto a 1/6 by 1/6 degree grid before we applied the algorithm (for more information see also Liu et al. 2012). If an eddy is detected an eddy center is identified analog to the OW-method as maximum (anticyclone) or minimum (cyclone) of SLA within the identified eddy structure.

When applying the two different eddy detection methods to the SLA data from the TANWA region, we used the same eddy detection thresholds for both methods, i.e. a feature only counts as an eddy, if its radius is larger than 45 km and it is detectable for a period of more than 7 days. Note, as the identified eddy areas are rarely circular we used the circle-equivalent of the area of the detected features to estimate the radius. For eddy tracking both eddy detection methods use the same tracking algorithm. An eddy trajectory was calculated if an eddy with the same polarity was found at least in 7 consecutive SLA maps (corresponding to one weeks) within a search radius of up to 50 km. Due to e.g. errors in SLA mappings (insufficient altimetric coverage) an eddy could vanish and reemerge after a while. Therefore we searched in 14 consecutive SLA maps (corresponding to 2 weeks) in a search radius of up to 100 km after an eddy disappearance, if eddies with the same polarity reemerges. If more than one eddy with the same polarity emerge within the search radius, we defined the following similarity parameter to discriminate between these eddies:

$$X = \sqrt{\left(\frac{\text{distance}}{100}\right)^2 + \left(\frac{\Delta \text{radius}}{\text{radius}_0}\right)^2 + \left(\frac{\Delta \text{vorticity}}{\text{vorticity}_0}\right)^2 + \left(\frac{\Delta \text{EKE}}{\text{EKE}_0}\right)^2}, \quad (1)$$

which include four terms based on the distance between the disappeared and newly emerged eddies and the difference of their radii, mean vorticities and mean eddy kinetic energy (EKE).  $\text{Radius}_0$ ,  $\text{vorticity}_0$  and  $\text{EKE}_0$  are the mean radius, vorticity and EKE of all identified eddies in TANWA. The newly emerged eddy with the smallest  $X$  is selected to be the same eddy. To give an idea of the uncertainty related to the detection technique both methods are

Florian Schütte 11.4.16 15:06

**Gelösch:** In order to detect and track eddy-like structures two different methods are applied to the SLA data. The first method, the Okubo-Weiß-Method (OW-method; Okubo (1970), Weiss (1991)), has been frequently used to detect eddies using satellite data as well as output from numerical studies (e.g. Isern-Fontanet et al. (2006), Chelton et al. (2007), Sangrà et al. (2009)). The basic assumption behind the OW-method is that regions where the relative vorticity dominates over the strain, i.e. where rotation dominates over deformation, characterize an eddy. In order to separate strong eddies from the weak background flow field a threshold needs to be identified. For this study the threshold is set to  $W_0 = -0.2 \cdot \sigma$ , where  $\sigma$  is the spatial standard derivation of the Okubo-Weiß parameter  $W = s_n^2 + s_s^2 - \omega^2$ . Here,  $s_n = \frac{\partial u}{\partial x} - \frac{\partial v}{\partial y}$  is the normal strain,  $s_s = \frac{\partial v}{\partial x} + \frac{\partial u}{\partial y}$  is the shear strain and  $\omega = \frac{\partial v}{\partial x} - \frac{\partial u}{\partial y}$  is the relative vorticity. A similar definition of the threshold was used in other eddy studies applying the OW-method (e.g. Chelton et al. (2007)).

Florian Schütte 11.4.16 14:33

**Formatiert:** Abstand Vor: Automatisch, Nach: Automatisch, Absatzkontrolle, Adjust space between Latin and Asian text, Adjust space between Asian text and numbers, Tabstopps bei: Nicht an 0,99 cm + 1,98 cm + 2,96 cm + 3,95 cm + 4,94 cm + 5,93 cm + 6,91 cm + 7,9 cm + 8,89 cm + 9,88 cm + 10,86 cm + 11,85 cm

Florian Schütte 11.4.16 14:32

**Gelösch:** When applying the methods to the TANWA region, we had to define eddy detection thresholds, i.e. a feature only counts as an eddy, if its radius is larger than 45 km and it is detectable for a period of more than 7 days. Note, as identified eddy areas are rarely circular we used the circle-equivalent of the area of the detected features to estimate the radius. An eddy trajectory was calculated if an eddy with the identical polarity and similar properties (deflection, radius, intensity, propagation direction) was found at least in 14 consecutive SLA maps (corresponding to two weeks) within the defined search radius of 10 (up to 60) km.

1 applied to the data. Every step is computed separately with both methods and the results are  
2 compared.

### 4 2.1.3 Eddy classification and associated mean spatial surface pattern

5 From the geostrophic velocity data anticyclones (cyclones) can be identified due to their  
6 negative (positive) vorticity. In the SLA data anticyclones (cyclones) are associated with a  
7 surface elevation (depression). The maximum (minimum) SLA marks the eddy center. In  
8 general, anticyclones (cyclones) carry enhanced (reduced) SST and enhanced (reduced) SSS  
9 in their cores, respectively. However, we found that 20% of all detected anticyclones had cold  
10 anomalies in their cores and a reduced SSS. This kind of eddies is classified as anticyclonic  
11 mode-water eddies (ACMEs) or intrathermocline eddies (Kostianoy and Belkin, 1989) as will  
12 later be confirmed when considering the in-situ observations (see below). Given that ACMEs  
13 show distinct characteristics, which are contrasting to anticyclones (see below), we  
14 distinguish in the following three types of eddies: anticyclones, cyclones and ACMEs.

15 Composites of satellite derived SST and SSS anomalies, with an extent of 300 km x 300 km  
16 around the eddy centers yield the mean spatial eddy surface pattern of temperature and  
17 salinity for the respective eddy type. The information whether an eddy is cold/warm or  
18 fresh/saline in the core is obtained by subtracting the average value over the edge of the box  
19 from the average value over the eddy center and its closest neighboring grid points. To  
20 exclude large-scale variations in the different datasets, the SST and SSS fields are low-pass  
21 filtered with cutoff wavelength of 15° longitude and 5° latitude. Thereafter the filtered  
22 datasets are subtracted from the original datasets thus preserving the mesoscale variability.  
23 The composite plots are based only on eddies with a radius between 45-70 km and an absolute  
24 SLA difference between the eddy center and the mean along the edge of the 300 km x 300 km  
25 box used for the composites greater than 2 cm.

## 27 2.2 In-situ Data

### 28 2.2.1 Argo Floats

29 A set of irregular distributed vertical CTD profiles was obtained from the autonomous  
30 profiling floats of the Argo program. The freely available data was downloaded from the  
31 Global Data Assembly Centre in Brest, France (www.argodatamgt.org) and encompasses the

Florian Schütte 5.4.16 12:04

**Gelöscht:** and the

Florian Schütte 5.4.16 12:06

**Gelöscht:** result

Florian Schütte 5.4.16 12:04

**Gelöscht:** s

Florian Schütte 12.4.16 10:18

**Gelöscht:** .

Florian Schütte 11.4.16 14:33

**Formatiert:** Englisch (USA)

Florian Schütte 12.4.16 12:09

**Gelöscht:** re

Florian Schütte 12.4.16 10:17

**Gelöscht:** .

Florian Schütte 11.4.16 15:11

**Formatiert:** Abstand Vor: Automatisch, Nach: Automatisch

Florian Schütte 22.4.16 11:41

**Gelöscht:** data

Florian Schütte 12.4.16 12:10

**Gelöscht:** re

Florian Schütte 1.4.16 15:19

**Gelöscht:** large scale

Florian Schütte 11.4.16 15:13

**Gelöscht:** The composite plots are based only on eddies with a radius between 45-70 km and an absolute SLA difference from the centre to the mean edge greater than 2 cm

Florian Schütte 12.4.16 10:18

**Gelöscht:** .

Florian Schütte 11.4.16 15:11

**Formatiert:** Schriftfarbe: Rot, Englisch (USA)

Florian Schütte 12.4.16 10:18

**Formatiert:** Abstand Vor: Automatisch, Nach: Automatisch, Absatzkontrolle, Adjust space between Latin and Asian text, Adjust space between Asian text and numbers, Tabstopps bei: Nicht an 0,99 cm + 1,98 cm + 2,96 cm + 3,95 cm + 4,94 cm + 5,93 cm + 6,91 cm + 7,9 cm + 8,89 cm + 9,88 cm + 10,86 cm + 11,85 cm

1 | period from July 2002 to December 2013. Here only pressure (P), temperature (T) and salinity  
2 | (S) data flagged with Argo quality category 1 are used. The given uncertainties are  $\pm 2.4$  dbar  
3 | for pressure,  $\pm 0.002$  °C for temperature and  $\pm 0.01$  for uncorrected salinities. In most cases the  
4 | salinity errors are further reduced by the delayed-mode correction. For this analysis an  
5 | additional quality control is applied in order to eliminate spurious profiles and to ensure good  
6 | data quality in the upper layers. [In the following, we give the criteria applied to the Argo float  
7 | profiles and in brackets the percentage, to which the criteria were fulfilled. Selected profiles  
8 | must i\) include data between 0 and 10 m depth \(98.2%\), ii\) have at least 4 data points in the  
9 | upper 200 m \(98.8%\), iii\) reach down to 1000 m depths \(95%\), iv\) continuous and consistent  
10 | temperature, salinity and pressure data \(78%\). This procedure reduced the number of profiles  
11 | by around 30% to 2022 Argo float profiles for the TANWA.](#)  
12

Florian Schütte 22.4.16 11:42

Gelöscht: ,

Florian Schütte 22.4.16 11:42

Gelöscht: ,

### 13 2.2.2 Shipboard measurements

14 In-situ CTD profile data collected during 20 ship expeditions to the TANWA within the  
15 framework of different programs is used (Figure 2b; see Table 1 for further details). In total  
16 | 579 profiles were available taken within [the](#) TANWA during the period March 2005 to June  
17 | 2013. Data sampling and quality control followed the standards set by GO-SHIP (Hood et al.,  
18 | 2010). However, we assume a more conservative accuracy of our shipboard data of about  
19 | twice the GO-SHIP standard, which is  $0.002$ °C and  $0.004$  for temperature and salinity,  
20 | respectively.  
21

Florian Schütte 11.4.16 14:28

**Gelöscht:** In particular, selected profiles must i) have the uppermost measurement between 0 and 10 m depth, ii) have at least 4 measurements in the upper 200 m, iii) have measurements down to 1000 m depths. This procedure reduces the number of profiles by 40% to 2022 Argo float profiles for the TANWA.

### 22 2.2.3 CVOO Mooring

23 The third set of in-situ data stems from the Cape Verde Ocean Observatory (CVOO) mooring.  
24 The CVOO mooring is a deep-sea mooring deployed at a depth of about 3600 m, 60 km  
25 northeast of the Cape Verdean island of São Vicente (Figure 2b). The nominal mooring  
26 position is  $17^{\circ}36'N$ ,  $24^{\circ}15'W$ . The mooring was first deployed in June 2006 and has been  
27 redeployed in March 2008, October 2009, May 2011 and October 2012. Temperature und  
28 salinity measurements in the upper 400 m have been typically recorded at depth of 30 m, 50  
29 m, 70 m, 100 m, 120 m, 200 m, 300 m and 400 m using MicroCAT instruments. Data  
30 | calibration is done against shipboard CTD data during the service cruises. [The uncertainties  
31 | are  \$\pm 0.002\$  °C for temperature and  \$\pm 0.01\$  for salinity.](#)

32 The eddy detection methods identifies 22 eddies passing the CVOO mooring. For these eddy  
33 events, the original time series with a temporal resolution of 15 or 20 minutes were low-pass  
34 | filtered with a [cut-off](#) period of 24 hours and consecutively subsampled to 1-day values in

Florian Schütte 11.4.16 16:27

Gelöscht: cutoff

1 order to reduce instrument noise and to match the resolution of the SLA maps. In total 429  
2 profiles could be obtained. T/S anomaly profiles were derived as the difference of profiles  
3 inside and outside of the eddies. The outside profiles were taken shortly before the eddy  
4 passage.

5

### 6 2.3 Determining the vertical structure of eddies detected in SLA data

7 In order to investigate the vertical structure of eddies identified in SLA data a combination of  
8 all available in-situ data sets was used. We had a total of 3030 CTD profiles available for the  
9 time period 2002 to 2013, with about 67% Argo float profiles, 19% shipboard CTD profiles  
10 and 14% mooring-based profiles (Figure 3). All profiles were vertically interpolated or re-  
11 gridded to 1 m vertical resolution in the depth range 5 to 1000 m. Missing data points within  
12 the first few meters of the water column were filled by constant extrapolation. For each  
13 profile, we determined the mixed layer depth (MLD) as the depth where the in-situ  
14 temperature decreased by 0.2 °C relative to 10m depth (de Boyer Montégut et al., 2004).

15 By co-location, in space and time, of eddies, that are identified in the SLA data using a  
16 combination of the OW and the GEO-method (an eddy has to be identified by both  
17 algorithms), with the combined in-situ data set, the vertical structures of anticyclones and  
18 ACMEs (positive SLA) and cyclones (negative SLA), were assessed (Figure 4). The  
19 classification results in 675 profiles taken in anticyclones/ACMEs, 499 profiles taken in  
20 cyclones and 1856 profiles taken outside of detected eddies. Excluding the mooring based  
21 profiles, from which we only extracted eddy events, around ~29% of all profiles (Argo float  
22 and shipboard CTD profiles) were taken coincidentally inside of an eddy. This proportion is  
23 in the range of earlier results derived by Chaigneau et al. (2011), who estimated that ~23% of  
24 their Argo float profiles in the eastern upwelling regions of the Pacific Ocean are conducted  
25 in eddies and Pegliasco et al. (2015), who found 38% of all their Argo floats profiles in the  
26 eastern upwelling areas conducted in eddies. We could also confirm the result of Pegliasco et  
27 al. (2015) that the majority of all Argo float profile in eddies are conducted in long-lived  
28 anticyclones/ACMEs.

29 However, we are interested in the anomalous water mass characteristic inside the eddy  
30 compared to the surrounding water. Anomaly profiles of potential temperature,  $\theta$ , salinity,  $S$ ,  
31 and potential density,  $\sigma_\theta$ , were derived as the difference of the profiles inside and reference  
32 profiles outside of an eddy. Profiles outside of eddies are required to be taken within a  
33 maximum distance of 120 km from the eddy center and at maximum  $\pm 25$  days apart from the  
34 time the profile inside of the eddy was taken (Figure 4). For 176 profiles out of the 1174

- Florian Schütte 22.4.16 12:04  
**Gelöscht:** both algorithms are required to identify an eddy
- Florian Schütte 22.4.16 12:03  
**Gelöscht:** and
- Florian Schütte 22.4.16 12:07  
**Gelöscht:** within
- Florian Schütte 22.4.16 12:07  
**Gelöscht:** ionically
- Florian Schütte 22.4.16 12:07  
**Gelöscht:** ically
- Florian Schütte 22.4.16 12:07  
**Gelöscht:** rotating eddies
- Florian Schütte 22.4.16 12:07  
**Gelöscht:** as
- Florian Schütte 22.4.16 12:21  
**Gelöscht:** of the eddies in anticyclones and cyclones is done with respect to the relative vorticity,
- Florian Schütte 22.4.16 12:21  
**Gelöscht:** ing
- Florian Schütte 11.4.16 15:18  
**Gelöscht:** Excluding the mooring based profiles, where we only extract eddy events, around ~29% of all profiles (Argo float and shipboard CTD profiles) were taken per coincidence inside of an eddy. This proportion is consistent with the results of Chaigneau et al. (2008), who estimate that ~25% of the eastern upwelling regions in the Pacific Ocean are covered by eddies.

1 | profiles inside of eddies no reference profile could be found fulfilling these criteria. In total  
2 | 587 anomaly profiles for anticyclones/ACMEs and 411 anomaly profiles for cyclones were  
3 | derived. As mentioned before it was useful to further separate anticyclonically rotating eddies  
4 | into two types: conventional anticyclones with downward bending isopycnals (and isotherms)  
5 | throughout and ACMEs with upward bending isopycnals in the upper 50 to 100 m depth and  
6 | downward bending isopycnals below. As a consequence, the MLD inside the ACMEs is  
7 | shallower compared to background values, while it can be several tens of meters deeper in  
8 | conventional anticyclones. We used the MLD difference to proof the separation into  
9 | conventional anticyclones and ACMEs from the satellite based surface signatures, described  
10 | above. In all cases, where the MLD inside of an anticyclonically rotating eddy was at least  
11 | 10 m shallower than the MLD outside the eddy, the eddy was associated with a negative SST  
12 | anomaly. Hence, the eddy type separation through satellite based surface signatures appears to  
13 | be accurate. The separation identified 95 out of 587 profiles in anticyclonically rotating eddies  
14 | as being taken in ACMEs (Figure 5). Averaging all anomaly profiles for anticyclones,  
15 | cyclones and ACMEs yields mean anomaly profiles for potential temperature,  $\bar{\theta}'$ , salinity,  $\bar{S}'$ ,  
16 | and potential density,  $\bar{\sigma}_{\theta}'$ , for the three different eddy types. Profiles of available heat and salt  
17 | anomalies (AHA [ $\text{J m}^{-1}$ ] and ASA [ $\text{kg m}^{-1}$ ]) per meter on the vertical were then derived as:

$$AHA = \pi r^2 \rho C_p \bar{\theta}', \quad (1)$$

$$ASA = 0.001 \cdot \pi r^2 \rho \bar{S}', \quad (2)$$

19 |  
20 | where  $\rho$  is density (in  $\text{kg m}^{-3}$ ),  $C_p$  is specific heat capacity ( $4186.8 \text{ J kg}^{-1} \text{ K}^{-1}$ ), and  $r$  is the  
21 | mean radius. The factor 0.001 in (2) is an approximation to convert PSS-78 salinity to salinity  
22 | fractions (kg of salt per kg of seawater). These calculations are partly adapted from  
23 | Chaigneau et al. (2011), where AHA and ASA are computed for eddies in the East Pacific.  
24 | Integrating AHA and ASA per meter over the depth range 0 to 350 m, the  $AHA_{\text{total}}$  (in J) and  
25 |  $ASA_{\text{total}}$  (in kg) was obtained. The lower boundary of integration was chosen as below 350 m  
26 | no significant temperature and salinity anomalies could be identified for the composite eddies  
27 | of the three eddy types.

28 | Eddies that pinch off from the eastern boundary are expected to carry waters with SACW  
29 | signature westward into areas where waters with NACW signature prevail. To quantify the  
30 | amount of SACW carried by these eddies, we follow a method developed by Johns et al.  
31 | (2003) used to quantify the amount of water of southern hemisphere origin carried by North  
32 | Brazil Current rings. Accordingly the highest/lowest 10% of the salinity values on potential

Florian Schütte 22.3.16 10:36  
**Gelöscht:** Anomaly profiles of potential temperature,  $\theta$ , salinity,  $S$ , and potential density,  $\sigma_{\theta}$ , were calculated as the difference of the profiles inside and outside of eddies. Profiles outside of eddies are required to be taken within a maximum distance of 120 km from the eddy centre and at maximum 25 days apart from the time the profile inside of the eddy were taken (Figure 4). This is how 587 anomaly profiles for anticyclones/ACME's and 411 anomaly profiles for cyclones were obtained. -

Florian Schütte 22.4.16 12:23  
**Gelöscht:** -

Florian Schütte 22.4.16 12:23  
**Gelöscht:** -

Florian Schütte 22.4.16 12:23  
**Gelöscht:** which have

Florian Schütte 22.4.16 12:24  
**Gelöscht:** -

Florian Schütte 22.4.16 12:24  
**Gelöscht:** -

Florian Schütte 22.4.16 12:26  
**Gelöscht:** to

Florian Schütte 22.4.16 12:27  
**Gelöscht:** cold

Florian Schütte 22.4.16 12:27  
**Gelöscht:** -

Florian Schütte 22.4.16 12:32  
**Gelöscht:**  $\bar{\theta}'$ , salinity,  $\bar{S}'$ , and potential density,  $\bar{\sigma}_{\theta}'$ ,

Florian Schütte 22.4.16 12:33  
**Gelöscht:** - ... [2]

Florian Schütte 22.4.16 12:33  
**Gelöscht:**  $r2\rho$

Florian Schütte 22.4.16 12:33  
**Gelöscht:**  $Cp$

Florian Schütte 12.4.16 10:28  
**Gelöscht:**  $\theta'$ , (1) - ... [3]

Florian Schütte 22.4.16 12:34  
**Gelöscht:** neat

Florian Schütte 22.4.16 12:34  
**Gelöscht:** h



1 density surfaces were averaged to define the mean NACW/SACW characteristics in the  
2 region as function of potential density. The obtained characteristics were used to determine  
3 the percentage of SACW contained in any profile taken inside and outside of eddies.  
4 Anomaly profiles of SACW percentage as function of potential density were then calculated  
5 as the difference of the profiles inside and outside of eddies and were eventually transformed  
6 back into depth space using a mean density profile.

7 To illustrate mean anomalies in potential temperature, salinity, potential density and SACW  
8 percentage for each eddy type as a function of depth and radial distance, the available profiles  
9 were sorted with respect to a normalized distance, which is defined as the actual distance of  
10 the profile from the eddy center, divided by the radius of the eddy. The profiles were grouped  
11 and averaged onto a grid of 0.1 between 0 and 1 of the normalized radial distance. Finally the  
12 field was mirrored at zero distance, and a running mean over three consecutive horizontal grid  
13 points was applied.

#### 14 2.4 Determining the heat, salt and volume transport

15 The three-dimensional structures of composite cyclones, anticyclones and ACMEs produced  
16 out of the combination of altimetry data and all available profiles were used to estimate the  
17 relative eddy contribution to fluxes of heat, salt and volume in the TANWA. Here we chose to  
18 define enclosed areas with Area I representing the extended boundary current region, Area II  
19 the transition zone and Area III the subtropical gyre region. By multiplying the heat transport  
20 of the composite eddies with the amount of eddies dissolving during a year in a given area  
21 (corresponding to an flux divergence) a mean heat release (in  $W m^{-2}$ ) and a mean salt release  
22 (in  $kg m^{-2}$ ) was calculated. The mean heat release can be compared to the net atmospheric  
23 heat flux in the area here derived from the NOC Surface Flux Dataset (Berry and Kent, 2011).  
24 Using the volume of a composite eddy (defined by the mean radius and the depth range 0 to  
25 350 m) and the mean SACW percentage within the eddy, the total volume transport of SACW  
26 of cyclones, anticyclones and ACMEs was calculated.

27

Florian Schütte 12.4.16 12:10

Gelöscht: re

Florian Schütte 22.4.16 12:34

Gelöscht: profiles are

Florian Schütte 22.4.16 12:35

Gelöscht: long 0

Florian Schütte 7.4.16 09:27

Gelöscht: counting eddies

Florian Schütte 22.4.16 12:35

Gelöscht: due to composite

# 1 3. Results and Discussion

## 2 3.1 Eddy statistics from SLA data

3 The two eddy tracking methods applied to the SLA data detected ~2800 eddies over the 19  
4 years of analysed data (Table 2, Figure 6) with slightly more cyclones than  
5 anticyclones/ACMEs (6% more in the OW-method, 2% more in the GEO-method). Note, that  
6 the given number of eddies must be seen as lower limit due to the coarse resolution of the  
7 satellite products. All of the detected eddies are nonlinear by the metric  $U/c$ , where  $U$  is the  
8 maximum circumpolar geostrophic surface velocity and  $c$  is the translation speed of the eddy.  
9 A value of  $U/c > 1$  implies that fluid is trapped within the eddy interior (Chelton et al., 2011)  
10 and exchange with the surrounding waters is reduced. Many of the eddies are even highly  
11 nonlinear, with 60% having  $U/c > 5$  and 4% having  $U/c > 10$ .

12 Considering only the period after 1998, i.e. when our SST data set becomes available, a  
13 satellite data-based separation between anticyclones (positive SST anomalies) and ACMEs  
14 (negative SST anomalies) is possible. We found that about 20% of the anticyclonically  
15 rotating eddies are ACMEs. However, the number of ACMEs might be underestimated,  
16 because ACMEs are associated with a weak SLA signature and therefore more difficult to  
17 detect with the SLA-based algorithms. Also the nonlinearity of ACMEs is underestimated by  
18 using geostrophic surface velocity as they have a subsurface velocity maximum.

19 Although the GEO-method in general detects slightly more eddies than the OW-method (in  
20 total 75 eddies more, which is 2.7% more than the OW-method) the situation is different near  
21 the coastal area where the OW-method detects 30 eddies per year but the GEO-method only  
22 22 eddies per year. This results from the strong meandering of the boundary current, where  
23 meanders are sometimes interpreted as eddies by the OW-method due to the high relative  
24 vorticity. In contrast, the GEO-method uses closed streamlines and therefore does not detect  
25 meanders as eddies, which makes this method more suitable for eddy detection in coastal  
26 areas. The average eddy radius in the TANWA is found to be  $56 \pm 12$  km (given here as mean  
27 and standard derivation), with the GEO-method resulting in around 10 km larger radii but also  
28 with a four times higher standard deviation when compared with the OW-method. The  
29 difference in the standard deviation of the eddy radius derived from GEO and the OW-method  
30 is partly due to the identification of few very large eddies using the GEO-method, which is  
31 not the case for the OW-method. In general, the OW-method appears to be the more reliable  
32 tool for identifying the eddy surface area and the corresponding radius in the TANWA.

33 Both algorithms show that on average the anticyclones and ACMEs are larger and have a

Florian Schütte 22.4.16 12:37

Gelöscht: warm

Florian Schütte 22.4.16 12:37

Gelöscht: cold

Florian Schütte 22.4.16 12:37

Gelöscht: ,

Florian Schütte 22.4.16 12:37

Gelöscht: even

Florian Schütte 22.4.16 12:38

Gelöscht: ose eddies

Florian Schütte 22.4.16 12:38

Gelöscht: identifies

Florian Schütte 22.4.16 12:39

Gelöscht: it

Florian Schütte 22.4.16 12:39

Gelöscht: ,

Florian Schütte 22.4.16 12:39

Gelöscht: while

Florian Schütte 22.4.16 12:40

Gelöscht: has a tendency to identify



1 longer lifetime than the cyclones. The average westward propagation speed is  $3.00 \pm 2.5$  km  
2  $d^{-1}$  for all eddy types, which is on the order of the first baroclinic mode Rossby wave phase  
3 speed at that latitude range (Chelton et al., 1998). The average tracking period (or lifetime) of  
4 an eddy in the TANWA is 28 days with a high standard deviation of 28 days. The longest  
5 consecutive tracking period for a single eddy (found similar in both algorithms) was around  
6 280 days for an anticyclone, 180 days for a cyclone and 200 days for an ACME. However,  
7 most of the eddies were detectable for a period of 7 to 30 days. The number of eddies  
8 decreases rapidly with increasing tracking period (Figure 6). Note that the OW-method  
9 detects 450 eddies with a lifetime between 7-14 days, which is more than the GEO-method.  
10 However, for longer lifetimes the GEO-method detects more eddies than the OW-method. As  
11 the tracking procedure in both algorithms is the same, the GEO-method seems to be more  
12 reliable in identifying and following eddy like structures from one time step to another. The  
13 percentage of tracked anticyclones/ACMEs and cyclones is close to 50% for short tracking  
14 periods. For longer lifetimes anticyclonic eddies tend to dominate, this is also reflected in the  
15 slightly shorter mean lifetimes of cyclones compared to anticyclones. [The dominance of long-](#)  
16 [lived anticyclones is also shown in the observational studies of Chaigneau et al. \(2009\),](#)  
17 [Chelton et al. \(2011\) and theoretically suggested by Cushman-Roisin and Tang \(1990\). The](#)  
18 [latter authors showed that in an eddying environment anticyclonic eddies are generally more](#)  
19 [robust and merge more freely than cyclones producing long-lived eddies, while cyclones](#)  
20 [show a higher tendency to self-destruction.](#)

21 Note, that tracking of eddies in the TANWA is prone to errors in particular regarding the  
22 information about the eddies' lifetime. Some eddies disappear [in single](#) SLA maps, which is  
23 at least partly due to the separation of the satellite ground tracks (Chaigneau et al., 2008). In  
24 order to avoid losing an eddy, we search two weeks after its assumed disappearance within a  
25 defined radius for [an](#) eddy [with the same polarity \(see section 2.1.2\)](#). The fact that purest  
26 SACW, which in the TANWA occurs in the eastern boundary region, is found regularly in  
27 eddy cores at the CVOO mooring (~850 km offshore) (Karstensen et al., 2015) shows that  
28 long-lived eddies must exist in the TANWA. Hence, the eddy tracking algorithms  
29 underestimate the eddy lifetime and accordingly overestimate the amount of newly generated  
30 eddies.

31 This challenge for the eddy tracking algorithms in the TANWA is probably the reason why  
32 Chelton et al. (2011) and Chaigneau et al. (2009) could not detect many long-lived eddies in  
33 this area. Their definition of long-lived eddies requires eddies to be trackable for longer than  
34 112 days (Chelton et al., 2011) or 35 days (Chaigneau et al., 2009). With the adaption of the

Florian Schütte 11.4.16 15:20

Gelöscht: .

Florian Schütte 22.4.16 12:49

Gelöscht: between consecutive

Florian Schütte 22.4.16 13:35

Gelöscht: similar

Florian Schütte 22.4.16 13:35

Gelöscht: properties

1 method for the TANWA with the two weeks search radius as described above, eddy tracking  
2 has improved, however some eddies might still be lost. [In addition, the mean eddy lifetime of  
3 eddies in TANWA is underestimated due to the restriction of eddy trajectories at the northern,  
4 southern and western boundaries.](#)

### 6 **3.2 Generation areas and pathways**

7 To identify hot spots of eddy generation, the locations of the first detection of each eddy is  
8 counted in  $1^\circ \times 1^\circ$  boxes (Figure. 7). The OW-method and the GEO-method do not show a  
9 significantly different pattern, except near the coast, where the local maximum in the number  
10 of newly detected eddies is shifted slightly offshore for the GEO-method compared to the  
11 OW-method. However, the distribution shows that most eddies are generated in the coastal  
12 area along the shelf. Within this region the headlands of the coast seem to play an important  
13 role as about 9 newly detected eddies per year are found around Cap Vert (Senegal), about 4  
14 eddies per year off Saint-Louis (Senegal) and about 5 eddies per year off Cap Timris  
15 (Mauretania). At these spots the algorithms detect more than 70% of the newly detected  
16 eddies (18 out of 25) per year in the coastal area. Another location of high eddy generation is  
17 southeast of the Cape Verde Islands, especially south of the northwesternmost Island, Santo  
18 Antão with about 2 newly detected eddies per year and southwest of Fogo with about 5 newly  
19 detected eddies per year.

20 To identify the preferred eddy propagation pathways, the locations of eddy centers, which  
21 were tracked for longer than one month (35 days), were counted in  $1/6^\circ \times 1/6^\circ$  boxes over all  
22 time steps. The spatial distribution of eddy activity indeed shows some structures and eddies  
23 tend to move along distinct corridors westward, away from the coast into the open ocean  
24 (Figure 8) as also shown for the Canary Island region (Sangrà et al., 2009). The propagation  
25 pathways can be separately investigated for the different eddy types: Most of the anticyclones  
26 are generated along the coast south of Cap Timris, off Saint-Louis and north off Cap Vert.  
27 They propagate either north of  $18^\circ\text{N}$  from their generation areas westward into the open  
28 ocean or south of  $18^\circ\text{N}$  with a southward deflection offshore. Their mean westward  
29 propagation speed is  $3.05 \pm 2.15 \text{ km d}^{-1}$ . Other generation hotspots for anticyclones are  
30 around the Cape Verde Islands south of Santo Antão and south of Fogo. For cyclones the  
31 generation areas are more concentrated than for anticyclones. North of Cap Timris and off  
32 Cap Vert are the main hotspots near the coast. On their way westwards cyclones tend to have  
33 a northward deflection in their pathways. The hotspot for cyclone generation around the Cape  
34 Verde islands is west of Fogo. Cyclones have a mean westward propagation speed of  $2.9 \pm$

Florian Schütte 12.4.16 12:05

Gelöscht: Formation

Florian Schütte 22.4.16 13:37

Gelöscht: s

Florian Schütte 12.4.16 12:10

Gelöscht: re

1 2.15 km d<sup>-1</sup>. Although not significantly different, the larger westward propagation speed of  
2 anticyclones compared to cyclones does agree with theoretical considerations regarding the  
3 westward eddy drift on a beta-plane (Cushman-Roisin et al., 1990).

4 The main generation areas for ACMEs near the coast are north of Cap Timris and off Saint-  
5 Louis around 18°N. ACMEs generated north of Cap Timris tend to have a slightly southward  
6 deflection on their way westwards into the open ocean, whereas the eddies generated off  
7 Saint-Louis show no meridional deflection and propagate along ~18°N into the open ocean.  
8 Their mean westward propagation speed is 3.05 ± 2.1 km d<sup>-1</sup>. The main generation area of  
9 ACMEs near Cape Verde Islands is located south of the northwesternmost island Santo  
10 Antão.

11

### 12 3.3 Seasonal variability of eddy generation

13 While the two eddy detection methods differ mostly in the number of identified eddies close  
14 to the coast, the season of peak eddy [generation](#) is very stable for both methods. A  
15 pronounced seasonality with a maximum of newly formed eddies during boreal summer  
16 (June/July), is obtained from both methods (Figure 9). During April to June newly generated  
17 eddies are mostly cyclonic, while during October to December newly generated eddies are  
18 mostly anticyclonic (anticyclones plus ACMEs). These seasonal differences indicate different  
19 eddy generation mechanisms at play in the TANWA during the different seasons. Different  
20 mechanisms for the generation of eddies in eastern boundary upwelling regions have been  
21 proposed (e.g. Liang et al. (2012)). Barotropic and baroclinic instabilities of the near coastal  
22 currents (Pantoja et al., 2012) triggered by e.g. the passage of poleward propagating coastal  
23 trapped waves (Zamudio et al. (2001), Zamudio et al. (2007)), wind perturbations (Pares-  
24 Sierra et al., 1993) or interactions of the large-scale circulation with the bottom topography  
25 (Kurian et al., 2011) are the main processes identified for the eddy generation in eastern  
26 boundary upwelling regions. In the TANWA, the period of maximum eddy [generation](#)  
27 (June/July) is characterized by a strong near-surface boundary current, the MC (Lázaro et al.,  
28 2005) suggesting dynamic instabilities of the boundary current as an important generation  
29 mechanism. However, there is a difference in peak [generation](#) of cyclones and anticyclones.

30 [While the maximum generation of cyclones occurs in June during the acceleration phase of](#)  
31 [the MC, the seasonality of anticyclone generation is not as distinct with weaker maxima in](#)  
32 [July and at the end of the year.](#) The generation of ACMEs has the main peak in April to May,  
33 which is at the end of the upwelling season. During that period the PUC is [likely](#) getting  
34 unstable and vanishes later on (Barton, 1989).

Florian Schütte 12.4.16 12:03

**Gelöscht:** formation

Florian Schütte 12.4.16 12:02

**Gelöscht:** formation

Florian Schütte 12.4.16 12:03

**Gelöscht:** formation

Florian Schütte 11.4.16 14:36

**Gelöscht:** While the maximum formation of cyclones occurs in June during the acceleration phase of the MC, the maximum formation of anticyclones occurs in July. This is the period, when the MC is getting unstable as can be seen from SLA.

1 The seasonal peak in eddy occurrence appears to propagate westwards into the open ocean.  
2 To illustrate this, annual harmonics are fitted to the number of eddies detected per month in 2°  
3 | x 2° boxes (Figure 10). Note, that the phase of a box is only shown when the amplitude is  
4 larger than 2.5 eddies per box. After the main generation of cyclones in the coastal area in  
5 June, the eddies enter the open ocean in late boreal autumn, passing the Cape Verde Islands  
6 and the ventilated gyre regime north of the CVFZ in boreal winter/spring. As mentioned  
7 before anticyclones are generated one to a few months later at the coast (July and October,  
8 | November). They dominantly reach the open ocean in boreal winter and spring and  
9 accordingly pass the Cape Verde Islands and the ventilated gyre regime north of the CVFZ in  
10 late boreal spring and summer. Note, that the relatively clear signal of the annual harmonic of  
11 eddy detections (Figure 10) also suggests that eddies with lifetime > 9 months are more  
12 frequent in the TANWA than indicated by the statistical output of the algorithms.

### 13 3.4 Mean eddy structure

#### 14 3.4.1 Surface anomalies related to eddies

15 For the three types of eddies, composites were constructed from daily SLA, SST, and SSS  
16 | anomaly fields. An area of 300 km x 300 km around every identified eddy center, (center =  
17 maximum value of SLA) was considered (Figure 11). Overall we had about 40.000 snapshots  
18 | of eddies between 1993 and 2013 available to calculate the mean SLA and SST anomalies. To  
19 derive mean SSS anomalies, only about 10.000 snapshots were merged because of the shorter  
20 time period of the SSS satellite data record (2010-2013).

21 For anticyclones, we found a positive SLA (maximum value in the eddy core is 6.9 cm  
22 (3.02 cm; 11.01 cm), given here as mean and the upper and lower limits of the 68% quartile  
23 range), a positive SST anomaly (maximum value in the eddy core 0.13 °C (0.03 °C; 0.24 °C))  
24 and a positive SSS anomaly (maximum value in the eddy core is 0.20 (-0.04; 0.52)). For  
25 cyclones, we found a negative SLA (minimum value in core -5.5 cm (-1.57 cm; -7.37 cm), a  
26 negative SST anomaly (minimum value in the core is -0.15 °C (-0.04 °C; -0.30 °C)) and a  
27 negative SSS anomaly (minimum value in the core is -0.16 (0.08; -0.48)). However, for the  
28 ACMEs (about 20% of the anticyclones) we found a negative SST anomaly (minimum value  
29 in the core is -0.15 °C (-0.04 °C; -0.31 °C) was observed. The vertical structure of these  
30 anticyclones as obtained from temperature and salinity profiles revealed the characteristic  
31 pattern of ACMEs with a very shallow mode in the upper 100 m or so. ACMEs also have a  
32 negative SSS anomaly (minimum value in the core is -0.13 (0.10; -0.33)). For all eddy types,  
33 SST dominates sea surface density.

34 Compared to SLA and SST measurements, the satellite-based observations of SSS are

Florian Schütte 22.4.16 13:40

Gelösch: anomaly

Florian Schütte 12.4.16 11:26

Gelösch: re

Florian Schütte 12.4.16 11:26

Gelösch: re

Florian Schütte 22.4.16 13:40

Gelösch: and SLA

1 | afflicted with high uncertainties and large measuring gaps. However, in the composite it is  
2 | possible to detect eddy type dependent anomalies, even if they are not as clear and circular  
3 | than the SLA and SST anomalies. The zonally stretched structures in the composites of SSS  
4 | anomalies may also result from the coarser temporal resolution of SSS data (i.e. 10 days)  
5 | resulting in a smearing of the eddy signal in the direction of propagation. Note, that the  
6 | composites of SSS anomalies showed only coherent eddy structures when selecting energetic  
7 | eddies (i.e., with a radius between 45-70 km and an absolute SLA anomaly >2 cm). The  
8 | composites of SLA and SST anomalies are much less affected by the restriction with regard to  
9 | the eddy amplitude.

Florian Schütte 22.4.16 13:41  
Gelöscht: SSS

10 |  
11 | In summary, the absolute SST and SSS anomalies of all three eddy types are of similar  
12 | magnitude. The magnitude of absolute SLA of anticyclones and cyclones is also somehow  
13 | similar, while ACMEs have a weaker SLA signature (which makes them more difficult to be  
14 | detected and tracked by satellite altimetry). The maximum surface circumpolar velocity is  
15 |  $0.18 \pm 0.12 \text{ m s}^{-1}$  in cyclones,  $0.17 \pm 0.12 \text{ m s}^{-1}$  in anticyclones and  $0.16 \pm 0.10 \text{ m s}^{-1}$  in  
16 | ACMEs. Overall, cyclones are slightly smaller, rotate faster and therefore have a shorter  
17 | lifetime than the other eddy types.

Florian Schütte 11.4.16 15:15  
Gelöscht:

### 19 | 3.4.2 Vertical structure of eddies

20 | Profiles from Argo floats, shipboard CTD and moorings were used to derive a mean vertical  
21 | eddy structure. Here, we calculated anomaly profiles of potential temperature, salinity and  
22 | potential density derived from profiles inside and outside of eddies. The mean vertical  
23 | structure and the anomalies presented here (Figure 12) are based on 492 profiles in  
24 | anticyclones, 411 profiles in cyclones but only 95 profiles in ACMEs. Consequently, the  
25 | statistics for ACMEs are weakest and the mean vertical structure must be interpreted with  
26 | care. Cyclones, anticyclones and ACMEs are characterised by a different  
27 | shallowing/deepening of isopycnal surfaces. Anticyclones carry a warm and saline water  
28 | anomaly, whereas cyclones and ACMEs host cold and less saline water in their cores. The  
29 | effect of temperature anomalies on density anomalies dominates over the effect of salinity  
30 | anomalies, which results in a positive density anomaly associated with cyclones (shoaling of  
31 | isopycnals) and a negative density anomaly associated with anticyclones (deepening of  
32 | isopycnals). This is illustrated by the elevation (deepening) of 25 m (36 m) of the density  
33 | surface of  $26.2 \text{ kg m}^{-3}$  in the core of the cyclone (anticyclone) compared to the surroundings.

Florian Schütte 22.4.16 13:43  
Gelöscht: fully

1 Due to the specific vertical structure of ACMEs, characterized by a strengthening of the  
2 anticyclonic rotation with depth in its upper part and a weakening of the anticyclonic rotation  
3 in its lower part, the ACMEs have a positive density anomaly in about the upper 100 m  
4 (shoaling of isopycnals) and a negative density anomaly below down to about 350 m  
5 (deepening of isopycnals). The mode-water in the core of the ACMEs is only weakly  
6 stratified. This is illustrated by the elevation of 48 m of the density surface of  $26.2 \text{ kg m}^{-3}$   
7 slightly above the core and the deepening of 52 m of the density surface of  $26.7 \text{ kg m}^{-3}$  below  
8 the core compared to the surroundings. From the mean vertical eddy profiles, we diagnose a  
9 maximum temperature anomaly underneath the mean mixed layer depth, which is at depth of  
10 about 50m. It is  $-2.42 \pm 1.23 \text{ }^\circ\text{C}$  at 55 m for cyclones and  $+1.88 \pm 1.37 \text{ }^\circ\text{C}$  at 54 m for  
11 anticyclones. The maximum salinity anomaly is  $-0.34 \pm 0.25$  at 70 m depth for cyclones and  
12  $+0.25 \pm 0.2$  at 100 m for anticyclones and as such located below the maximum temperature  
13 anomaly. The respective maximum density anomalies are, as expected, close to the location of  
14 the maximum temperature anomaly, and are  $0.28 \pm 0.42 \text{ kg m}^{-3}$  at 48 m for cyclones and  $0.44$   
15  $\pm 0.35 \text{ kg m}^{-3}$  at 50 m for anticyclones. The mean ACME structure is characterized by a much  
16 stronger temperature anomaly of  $-4.0 \pm 2.2 \text{ }^\circ\text{C}$  at 51 m depth and salinity anomaly of  $0.72 \pm$   
17  $0.38$  at 74 m depth in comparison to cyclones and anticyclones. Note, that the cold and fresh  
18 SACW in the ACME core does not produce a positive temperature anomaly when it reaches  
19 deeper levels due to the downward bending of isopycnal surfaces below the eddy core. The  
20 ACME density anomaly has a maximum of  $0.66 \pm 0.35 \text{ kg m}^{-3}$  at about 47 m and a minimum  
21 of  $-0.08 \pm 0.06 \text{ kg m}^{-3}$  at about 168 m, which reflects the shoaling and deepening of  
22 isopycnals towards the eddy center above and below its core. Note, that below the eddy core  
23 (>150 m depth) horizontal density anomalies are dominated by salinity with temperature  
24 playing a minor role. For all eddy types, cyclones, anticyclones and ACMEs, temperature,  
25 salinity and density anomalies reach down to about 300-350 m depths with a maximum  
26 beneath the mixed layer or slightly deeper.

27 Chaigneau et al. (2011) observed mean maximum anomalies of  $\pm 0.7 \text{ }^\circ\text{C}$  in temperature and  $\pm$   
28  $0.06$  in salinity based on Argo float measurements in eddy cores within the Southeast Pacific.  
29 For the TANWA the mean maximum anomalies of about  $\pm 2 \text{ }^\circ\text{C}$  in temperature and  $\pm 0.3$  in  
30 salinity are more than twice as high. The presence of different water masses, cold and fresh  
31 SACW prevailing in the coastal region and warmer and saltier NACW further offshore,  
32 results in the large temperature and salinity anomalies in eddy cores in the TANWA  
33 compared to the Southeast Pacific. Furthermore the reference used for calculating an anomaly  
34 can create large differences. Chaigneau et al. (2011) computed the anomalies of Argo float

Florian Schütte 22.4.16 13:46

**Gelöscht:** However, as said before, the mean ACME structure is based on less independent measurements than for the other eddy types.

Florian Schütte 12.4.16 12:11

**Gelöscht:** re

Florian Schütte 29.3.16 19:32

**Gelöscht:**

Florian Schütte 22.4.16 13:46

**Gelöscht:** ies

Florian Schütte 7.4.16 09:55

**Formatiert:** Englisch (USA)

Florian Schütte 12.4.16 11:34

**Formatiert:** Absatzkontrolle, Adjust space between Latin and Asian text, Adjust space between Asian text and numbers, Tabstopps bei: Nicht an 0,99 cm + 1,98 cm + 2,96 cm + 3,95 cm + 4,94 cm + 5,93 cm + 6,91 cm + 7,9 cm + 8,89 cm + 9,88 cm + 10,86 cm + 11,85 cm

1 profiles relative to interpolated climatological profiles taken from CSIRO Atlas of Regional  
2 Seas (CARS). Here, we tested five different references to calculate anomalies and found  
3 significantly different anomalies, even with reversed sign (Table 3). The differences in the  
4 mean anomalies depend on the used reference profiles. Besides the “next profile outside”, we  
5 used different climatologies as reference. However, differences in temperature and salinity  
6 between the different climatologies are of similar magnitude than the derived mean anomalies  
7 of the different eddy types (Table 1). When using the “next profile outside” as reference we  
8 obtained larger mean anomalies, which could suggest that the “next profile outside” is  
9 systematically biased by nearby eddies of reversed polarity (which are possibly not well  
10 identified by the eddy detecting methods). However, in particular in regions with strong  
11 gradients/fronts (e.g., CVFZ, coastal upwelling) with strong seasonality and variability, the  
12 “next profile outside” should deliver the most realistic background condition surrounding an  
13 eddy and thus should be preferably used to calculate water mass anomalies transported by  
14 eddies.

15 Here, we want to note that the uppermost data point (at 5 m) of the mean temperature and  
16 salinity anomaly profiles of the three types of eddies from the selected in-situ data (Figure 12)  
17 agrees well with the surface anomalies based on satellite data composites (Figure 11) and  
18 amounts to maximum values of -0.15 °C (in-situ: -0.15 °C) for cyclones, 0.13 °C (in-situ:  
19 0.25 °C) for anticyclones and -0.15 °C (in-situ: -0.20 °C) for ACMEs; corresponding salinity  
20 anomalies are -0.16 (in-situ: -0.10) for cyclones, 0.2 (in-situ: 0.13) for anticyclones and -0.13  
21 (in-situ: -0.11) for ACMEs.

### 23 3.5 Contribution of eddies to zonal transport of properties

#### 24 3.5.1 Thermohaline content and associated transport of eddies

25 For all cyclones/anticyclones/ACMEs a mean eddy volume of  $2.860 \times 10^{12} \text{ m}^3 / 3.089 \times 10^{12} \text{ m}^3$   
26  $/ 2.973 \times 10^{12} \text{ m}^3$  is derived, considering their mean radii (51 km/53 km/52 km) and a mean  
27 depth of 350 m for all three eddy types. Distributed over a period of one year this leads to a  
28 westward volume flux associated with a single eddy of about 0.1 Sv.

29 The mean three-dimensional structure of temperature and salinity anomalies associated with  
30 cyclones, anticyclones and ACMEs (Figure 12) was used to estimate profiles of AHA and  
31 ASA per meter (Figure 13). The maximum AHA per meter is located at depths comparable to  
32 the maximum temperature anomaly and at about 55 m for all eddy types. The maximum ASA  
33 per meter is located deeper at about 80 m depth (~70 m depth for cyclones, ~80 m for ACMEs  
34 and ~110 m for anticyclones). The  $AHA_{\text{total}}$  ( $ASA_{\text{total}}$ ), derived by integrating the profiles of

Florian Schütte 29.3.16 15:25

**Gelöscht:** We subtract the nearest profile in time and space (within 120 km distance and 25 days) outside of an eddy from the profile inside of the eddy, which results in the most realistic dynamic anomaly of the eddy with respect to the actual background water mass. However, this is only possible if enough profiles are available.

Florian Schütte 12.4.16 11:34

**Formatiert:** Englisch (USA)

Florian Schütte 22.4.16 13:50

**Gelöscht:** T

Florian Schütte 22.4.16 13:51

**Gelöscht:** surprisingly

Florian Schütte 22.4.16 13:51

**Gelöscht:** s

Florian Schütte 22.4.16 13:51

**Gelöscht:** s



1 AHA (ASA) per meter from the surface to 350 m, is  $-14.5 \times 10^{18}$  J ( $-73.0 \times 10^{10}$  kg) for  
2 cyclones,  $11.0 \times 10^{18}$  J ( $40.7 \times 10^{10}$  kg) for anticyclones and  $-15.4 \times 10^{18}$  J ( $-94.2 \times 10^{10}$  kg)  
3 for ACMEs (see also Table 4).

4 Comparing our results to the Southeast Pacific (cyclones:  $AHA_{total}=-5.5 \times 10^{18}$  J,  
5  $ASA_{total}=-9.8 \times 10^{10}$  kg; anticyclones:  $AHA_{total}=8.7 \times 10^{18}$  J,  $ASA_{total}=23.8 \times 10^{10}$  kg)  
6 (Chaigneau et al., 2011), we found an overall smaller volume of the eddies in the TANWA,  
7 but derived larger heat and salt anomalies. On the one hand this could be explained by the fact  
8 that we average over a smaller area. However, regional differences should also exist e.g.  
9 related to the boundary current hydrographic structure or the mean rotation speed (hence  
10 bending of isopycnals). For ACMEs in the Southeast Pacific there is only one recent estimate  
11 by Stramma et al. (2013) for comparison, who estimated the  $AHA_{total}$  and  $ASA_{total}$  of a well-  
12 observed ACME to be  $17.7 \times 10^{18}$  J and  $36.5 \times 10^{10}$  kg, respectively. The heat and salt  
13 anomalies are of the same order as found for the mean ACME in the TANWA but with  
14 reversed sign, which is remarkable. The ACME observed in the Southeast Pacific transports  
15 in contrast to the composite ACMEs in the TANWA warm and saline waters in its core  
16 offshore. One possible explanation is the different water mass characteristics in the source  
17 (coastal) region of the ACMEs in the Southeast Pacific compared to the TANWA.

18 Evenly distributed over a period of one year the heat (salt) transport associated with one  
19 single eddy is  $-4.6 \times 10^{11}$  W ( $-23.2 \times 10^3$  kg  $s^{-1}$ ) for cyclones,  $3.5 \times 10^{11}$  W ( $12.9 \times 10^3$  kg  $s^{-1}$ )  
20 for anticyclones, and  $-4.9 \times 10^{11}$  W ( $-29.9 \times 10^3$  kg  $s^{-1}$ ) for ACMEs. As expected from the  
21 lower  $AHA_{total}$  ( $ASA_{total}$ ) that has been derived for eddies in the Southeast Pacific (Chaigneau  
22 et al., 2011), the heat (salt) transport due to eddies in the TANWA is comparably large (see  
23 also Table 4).

24 In order to estimate the large-scale impact of the heat and salt transport by these eddies in the  
25 TANWA, we define three characteristic areas (see Figure 14): the extended boundary current  
26 region (Area I), the transition zone (Area II), and the subtropical gyre region (Area III). Based  
27 on the results from the GEO-method, 21 eddies are formed each year in the extended  
28 boundary current region of the TANWA. While about 5 eddies dissipate quickly and only  
29 influence the near coastal regions, about 16 eddies per year leave the extended boundary  
30 current region and propagate into the transition zone of the TANWA (Figure 14a). Based on  
31 the mean temperature and salinity anomalies derived above, it equates to a heat (salt)  
32 transport of  $-35.9 \times 10^{11}$  W ( $-180.6 \times 10^3$  kg  $s^{-1}$ ) by cyclones,  $23.0 \times 10^{11}$  W ( $85.3 \times 10^3$  kg  $s^{-1}$ )  
33 by anticyclones and  $-8.8 \times 10^{11}$  W ( $-53.8 \times 10^3$  kg  $s^{-1}$ ) by ACMEs. With regard to the number  
34 of eddies that dissolve in the different areas per year an “equivalent surface heat flux” (ESHF)

Florian Schütte 22.4.16 14:11

Gelöscht: more intense

Florian Schütte 12.4.16 11:39

Gelöscht: -

Florian Schütte 12.4.16 11:39

Gelöscht: -

Florian Schütte 22.4.16 14:13

Gelöscht: This is in general agreement with

Florian Schütte 12.4.16 11:44

Gelöscht: -

Florian Schütte 12.4.16 11:40

Gelöscht: E



1 is computed and compared with the annual mean net surface heat flux for the respective  
2 regions as taken from the NOC Surface Flux Dataset (Berry and Kent, 2011) (Figure 14b).

3 The anomalies in heat and salt associated with the three different types of eddies partly  
4 counteract each other. Anomalies in cyclones and ACMEs are negative, indicating heat and  
5 salt deficiencies in their core, while anomalies in anticyclones represent a surplus of heat and  
6 salt with respect to the background conditions. The cyclonic eddies provide an ESHF in Area  
7 II of about  $-3.0 \text{ W m}^{-2}$ , anticyclones of about  $+2.0 \text{ W m}^{-2}$ , and ACMEs of about  $-0.6 \text{ W m}^{-2}$ ,  
8 which results in a net ESHF associated with all eddies of about  $-1.6 \text{ W m}^{-2}$ . This heat flux due  
9 to eddies represents about 10% of the net surface heat flux in the transition zone of the  
10 TANWA that is about  $+17.4 \text{ W m}^{-2}$ .

11 In the open ocean of the TANWA, cyclones and ACMEs contribute to a cooling and  
12 freshening of the upper ocean and anticyclones to a warming and salinity increase. As such,  
13 the mesoscale eddy field and its seasonal to interannual variability can have an impact on the  
14 regional heat and salt budgets of the TANWA. However, because our calculations only  
15 account for long-lived eddies with a radius larger than 45 km, the calculated absolute eddy  
16 fluxes represent a lower limit that might increase when accounting also for short-lived, non-  
17 coherent eddies and/or sub-mesoscale variability.

### 19 3.5.2 Zonal eddy dependent westward transport of SACW

20 Many of the eddies that originate in the eastern boundary region carry water of South Atlantic  
21 origin westward. In order to quantify the SACW signature in the eddies, a water mass analysis  
22 was performed. For all isopycnals SACW (labelled 100%) and NACW (labelled 0%)  
23 temperature and salinity pairs were defined using extremes of all observational data (see  
24 Figure 2). Then the percentages of SACW concentrations contained inside the eddy cores  
25 were estimated. However, because the background field also transitions along the eddy  
26 trajectories towards stronger NACW characteristic, we estimated the SACW content of the  
27 eddies relative to the surrounding waters. Figure 15 shows the average vertical structure of the  
28 trapped SACW anomaly relative to the background for each eddy type. The different eddy  
29 types have a different potential in trapping SACW in their cores. Cyclones contain on average  
30 16% (maximum core value: 35%) more SACW than the surrounding water and ACMEs even  
31 21% (maximum core value: 60%). This implies a negative heat and salt anomaly along  
32 isopycnal layers inside of cyclones and ACMEs. Furthermore it shows the prominent  
33 capability of ACMEs to trap and isolate anomalous water inside their cores. In contrast, the  
34 SACW anomaly in anticyclones is weak and negative (on average -4%; minimum core value -

Florian Schütte 22.4.16 14:18

**Gelöscht:** Hence, the net contribution of mesoscale eddies to the heat and salt transport is probably weak.

Florian Schütte 22.4.16 14:19

**Gelöscht:** Area II

Florian Schütte 30.3.16 15:43

**Gelöscht:** 1

Florian Schütte 22.4.16 14:21

**Gelöscht:** d

Florian Schütte 22.4.16 14:21

**Gelöscht:** points out

1 10%), implying that anticyclones contain on average a positive heat and salt anomaly along  
2 isopycnal layers. As such, anticyclones counteract the westward transport of SACW  
3 associated with the propagation of cyclones and ACMEs. Anticyclones instead transport small  
4 amounts of NACW westward.  
5 To estimate an absolute transport of SACW from the eddy generation area at the eastern  
6 boundary into the open ocean, the mean percentages of SACW contained inside the different  
7 eddy types can be used. Highest percentage of SACW (>80%) is found in the extended  
8 boundary current region (Area I). Northwestward towards the open ocean the SACW  
9 percentage decreases (Area II ~ 57%, Area III < 23%; Figure 16b). Hence, when the eddies  
10 are generated in the extended boundary current region (in Area I) they trap waters with  
11 SACW signature in their cores and transport it westward into the open ocean (Area II and  
12 Area III), where waters with NACW signature prevail. These anomalous properties with  
13 respect to the surrounding waters can be visualized in a salinity versus sigma-theta diagram  
14 (Figure 16a). ACMEs exhibit the strongest SACW signature, indicating again that ACMEs  
15 have the best capability to trap water. The percentage of SACW in the different eddy types  
16 within the three separated areas are shown in the white circles in Figure 16b. Again the strong  
17 capability of ACMEs to transport SACW is obvious. In Area II (background ~57% SACW)  
18 ACMEs still exhibit 82% SACW and in Area III (background <23% SACW) it is 78%  
19 SACW, indicating that ACMEs are only weakly affected by lateral and vertical mixing.  
20 Cyclones contain 69% SACW in Area II and 52% SACW in Area III and as such lose SACW  
21 signature from their cores much faster. Anticyclones with 59% SACW in Area II and 29%  
22 SACW seem to have almost the same SACW signature as the background. This indicates that  
23 either they are not well isolated, and their cores are already replaced with the surrounding  
24 water, or that they are transporting low SACW signatures in their cores from the beginning.  
25 Using the number of eddies passing the boundaries of the areas and the “excess” percentage  
26 of SACW in their cores (relative to the background), an “eddy type dependent” absolute  
27 transport of SACW out of the boundary current was derived (Figure 16b). We obtained an  
28 absolute transport of 2.07 Sv of SACW out of the boundary current near the coast into the  
29 extended boundary current region (Area I) of which about 0.81 Sv of SACW reached the  
30 transition zone (Area II). Further to the west, about 0.36 Sv of SACW reached the subtropical  
31 gyre region west of the Cape Verde Islands (Area III). Considering the volume of the upper  
32 350 m of the transition zone (Area II,  $2 \times 10^5 \text{ km}^3$ ), the eddy transport will replenish the  
33 SACW part in about 2.5 years. Note, that these calculations represent conservative  
34 assumptions about the SACW transport since the contribution of short-lived, non-coherent

Florian Schütte 22.4.16 14:22

**Gelöscht:** Area I (the extended boundary current region) exhibits the

Florian Schütte 22.4.16 14:22

**Gelöscht:** h

Florian Schütte 22.4.16 14:23

**Gelöscht:** near the coast

Florian Schütte 22.4.16 14:24

**Gelöscht:** 15b

Florian Schütte 22.4.16 14:27

**Gelöscht:** (Area II, A= 208 880 km<sup>3</sup>)

1 and smaller scale eddies to the SACW transport is not included. For example, the highly  
2 energetic cyclone generated at the headland of Cap Vert discussed in detail by Alpers et al.  
3 (2013), which has a radius of 10 to 20 km and a Rossby number larger than one, is not  
4 detected by the eddy detection algorithms used in this paper due to its small scale, but  
5 certainly contributed to the westward transport of near-coastal water masses.  
6

Florian Schütte 22.4.16 14:28

Gelöscht: between

#### 7 4. Summary and Conclusion

8 Within this study we analysed satellite based remotely sensed data, including SLA, SST, SSS,  
9 as well as in-situ temperature and salinity profiles, taken from Argo floats, ships and  
10 moorings, in order to examine the eddy characteristics and dynamics in the TANWA. Eddies  
11 were identified based on their manifestation in SLA data using two different eddy detection  
12 algorithms, the OW-method and the GEO-method. Both detection algorithms produced rather  
13 similar results except for the open ocean/coastal transition zone, where the OW methods seem  
14 to overestimate the amount of eddies due to high vorticity values associated with the  
15 meandering boundary current.

16 We found that anticyclones (cyclones) are associated with enhanced (reduced) SLA, enhanced  
17 (reduced) SST and enhanced (reduced) SSS in their eddy cores, respectively. However, 20%  
18 of all [eddies with enhanced SLA](#) showed reduced SST and reduced SSS and we were able to  
19 classify these [eddies as](#) anticyclonic mode-water eddies (ACMEs). Of the average  $146 \pm 4$   
20 eddies detected per year in the TANWA over 19 years of SLA data, the ratio of cyclonic and  
21 anticyclonic eddies is nearly equal (52% cyclones, 39% anticyclones, 9% ACMEs), with a  
22 similar radius of  $56 \pm 12$  km for all three eddy types.

Florian Schütte 22.4.16 14:29

Gelöscht: detected anticyclones

Florian Schütte 22.4.16 14:30

Gelöscht: an anomalous

Florian Schütte 22.4.16 14:30

Gelöscht: anticyclones to be

23 In agreement with earlier findings (Chaigneau et al. (2009)) we found eddies being generated  
24 mainly near the coast and here at some topographic “hot spots”. For the TANWA these hot  
25 spots are associated with the headlands of Cap Vert (Senegal) and Cap Timris (Mauretania).  
26 We could also confirm the existence of a seasonality in the eddy generation (Chaigneau et al.  
27 (2009), Kurczyn et al. (2012)) and found cyclones form preferably during April to June, while  
28 anticyclones and ACMEs are mostly generated from October to December. After their  
29 generation, eddies of all three types propagate westward with a speed,  $c$ , of about  $3.00 \pm 2.15$   
30  $\text{km day}^{-1}$ , which is in general agreement with the first baroclinic mode Rossby wave phase  
31 speed at that latitude range (Chelton et al., 1998). We found that anticyclones/cyclones follow  
32 distinct corridors with a meridional deflection towards the equator/pole. This is in agreement  
33 with the theoretical and observational findings of the deflection from the  $\beta$ -drift of

Florian Schütte 22.4.16 14:31

Gelöscht: ic

Florian Schütte 22.4.16 14:31

Gelöscht: eddies (including ACMEs)

1 anticyclones and cyclones (Chelton et al., 2011). In contrast, ACMEs do not show a  
2 significant meridional deflection.

3

4 We suspect that the eddy generation is related to instabilities of the eastern boundary current.

5 Eddy generation resulting from interactions of coastal currents with headlands is a well-  
6 known process and has been extensively investigated (e.g. Røed (1980), Klinger (1994a),  
7 Klinger (1994b), Pichevin and Nof (1996), Crawford et al. (2002), Zamudio et al. (2007)).

8 Most likely the generation is driven by flow separation at the headlands of the West African  
9 coast, triggered by seasonality in the wind forcing. For the North-Eastern Pacific it has been

10 shown that coastal trapped waves have an impact on the stability of coastal currents and hence  
11 eddy generation (Zamudio et al. (2001), Zamudio et al. (2006), Zamudio et al. (2007)). Such

12 eddy generation mechanisms may explain the high eddy generation in the TANWA found  
13 during phases of strongest boundary current velocities. However, the detailed investigation of

14 the generation mechanisms of eddies in the TANWA requires realistic high-resolution  
15 modelling and is beyond the scope of the present study.

16 The maximum swirl velocity of the eddies,  $U$ , as obtained from the surface geostrophic  
17 velocity is about  $14.7 \pm 9.5 \text{ km day}^{-1}$  indicating a high nonlinearity of the observed eddies, i.e.

18  $U/c > 1$ . Due to this nonlinearity the exchange between eddy core and surrounding water is  
19 limited and hence they are able to trap water masses and transport them over large distances.

20 In the TANWA the eddies act as transport agents for SACW that is present in the eastern  
21 boundary upwelling region toward, and across the CVFZ into the subtropical gyre region,  
22 where NACW dominates.

23 In order to estimate the water mass anomalies transported by the different eddy types, their  
24 vertical water mass structures were estimated. Cyclones (anticyclones) are associated with

25 maximum temperature/salinity anomalies of about  $-2.42 \pm 1.23 \text{ }^\circ\text{C}$  /  $-0.34 \pm 0.25$  ( $1.88 \pm$   
26  $1.37 \text{ }^\circ\text{C}$  /  $0.25 \pm 0.2$ ), respectively, most intense just beneath the mixed layer in the depth

27 range 55 to 100 m. With respect to water mass anomalies the ACMEs stand out because their  
28 maximum absolute anomaly is more than twice as large (temperature anomalies of  $-4 \pm 2.2 \text{ }^\circ\text{C}$

29 and salinity anomalies of  $+0.72 \pm 0.38$ ) compared to the corresponding anomalies of cyclones  
30 or normal anticyclones. Moreover, their mixed layer depth is found at much shallower depth

31 of 40 to 70 m. Given the fundamentally different anomalies that are associated with the two  
32 types of eddies with anticyclonic surface flow (normal anticyclones and ACMEs), a separate

33 treatment of these eddy types seems to be mandatory when discussing eddy transports. This  
34 has not been done routinely in the past (e.g. Chaigneau et al. (2009), Zhang et al. (2014))

Florian Schütte 22.4.16 14:32

Gelöscht: in the near coastal

Florian Schütte 22.4.16 14:33

Gelöscht: In particular f

Florian Schütte 22.4.16 14:34

Gelöscht: are somehow coherent to our results with

Florian Schütte 22.4.16 14:34

Gelöscht: est

Florian Schütte 22.4.16 14:34

Gelöscht:

Florian Schütte 22.4.16 14:35

Gelöscht: interior (eddy)

Florian Schütte 22.4.16 14:35

Gelöscht: )

Florian Schütte 22.4.16 14:35

Gelöscht: y

Florian Schütte 22.4.16 14:37

Gelöscht: anticyclonic

1 primarily because SLA data alone does not provide the necessary information. Here, we were  
2 able to distinguish ACMEs from normal anticyclones by using SSS and SST data in parallel.  
3 The magnitude of the obtained anomalies varies according to the reference dataset  
4 (background data) being used. We tested nearby in-situ data collected outside of eddies as  
5 well as different climatological fields (Table 3) as e.g. in Chaigneau et al. (2009). Using the  
6 inferred temperature and salinity anomalies we were able to calculate the associated heat  
7 (salt) transports for the different eddy types. They amount to  $-4.6 \times 10^{11}$  W ( $-23.15 \times 10^3$  kg s<sup>-1</sup>)  
8 for cyclones,  $3.5 \times 10^{11}$  W ( $12.9 \times 10^3$  kg s<sup>-1</sup>) for anticyclones, and  $-4.9 \times 10^{11}$  W ( $-29.9 \times$   
9  $10^3$  kg s<sup>-1</sup>) for ACMEs. Out of the 21 eddies formed each year in the TANWA along the  
10 eastern boundary, 5 dissipate in a band of about 250 km width near the coast and about 16  
11 propagate into the open ocean adding up to an annual eddy net heat (salt) transport of about  
12  $50 \times 10^{11}$  W ( $-150 \times 10^3$  kg s<sup>-1</sup>). Converting the divergence of the heat transport in the  
13 transition zone (Area II) into an equivalent surface heat flux we found a cooling of the ocean  
14 of  $-1.6$  W m<sup>-2</sup> due to eddy heat transport, which as such balances about 10% of the net surface  
15 heat flux of  $17.4$  W m<sup>-2</sup> as obtained from the NOC Surface Flux Dataset (Berry and Kent,  
16 2011).

17 The TANWA is a crossroad for water masses, with NACW prevailing in the northwest within  
18 the ventilated subtropical gyre and SACW in the eastern boundary upwelling region. In order  
19 to estimate the dispersal of SACW due to eddies within the TANWA, we analysed the SACW  
20 content in the three different eddy types using the in-situ profile data. We found that cyclones  
21 contain on average about 16% more SACW than the surrounding water, ACMEs 21%, and  
22 normal anticyclones do not carry any SACW anomaly. Some ACMEs efficiently isolate their  
23 eddy cores from the surrounding waters reaching maximum SACW anomalies of more than  
24 60%, which indicates a high nonlinearity and coherence of these eddies (Karstensen et al.,  
25 2015).

26 Considering the total tracer transport of the eddies along isopycnals (spiciness), the negative  
27 heat and salt anomaly within cyclones and ACMEs results in a mean water mass transport of  
28 2.07 Sv of SACW out of the boundary current region, of which about 0.36 Sv of SACW reach  
29 the subtropical gyre region northwest of the Cape Verde Islands. Hence, the SACW transport  
30 due to eddies would renew the SACW part of the transition zone located between the  
31 extended eastern boundary region and the subtropical gyre region (assuming a layer thickness  
32 of 350 m) in about 2.5 years.

33 This study gives a first insight into the types and characteristics of eddies within the TANWA  
34 as well as in the fluxes of heat and salt associated with their westward propagation.

Florian Schütte 22.4.16 14:39

Gelöscht: are

1 Remaining open questions regard the importance of short-lived eddies for the transport of  
2 heat and salt (which could not be evaluated due to the resolution of the available data sets), as  
3 well as the individual processes responsible for eddy generation. The distinction of  
4 anticyclonic rotating eddies into ACMEs and “normal anticyclones” seems to be mandatory  
5 for future eddy studies as these two eddy types strongly differ in their efficiency to carry  
6 water mass anomalies. Moreover, the biogeochemical responses in ACMEs have been found  
7 to be very distinct from normal anticyclones and a sufficient representation of both types of  
8 anticyclones in coupled physical-biogeochemical models may be crucial for a realistic  
9 simulation of eastern boundary upwelling systems.

## 10 Acknowledgements

11 This study is funded by the Deutsche Bundesministerium für Bildung und Forschung (BMBF)  
12 as part of the project AWA (01DG12073E) and by the Deutsche Forschungsgemeinschaft as  
13 part of the Sonderforschungsbereich 754 “Climate – Biogeochemistry Interactions in the  
14 Tropical Oceans” and the project FOR1740 and through several research cruises with RV  
15 Meteor, RV Maria S. Merian, RV Poseidon and RV L’Atalante. We thank the captains and  
16 crew as well as all chief scientists and scientists of the involved research vessels and our  
17 technical group for their help with the fieldwork. Furthermore the authors thank Ping Chang,  
18 Rebecca Hummels, Tim Fischer and Robert Kopte for helpful discussions. For ship and  
19 mooring data processing we thank Gerd Krahnmann. In addition we thank the international  
20 Argo program and the national programs that contribute to it, which collected the data and  
21 made it freely available. The Argo program is part of the Global Ocean Observing System.  
22 The altimeter products were produced and distributed by *Aviso*  
23 (<http://www.aviso.altimetry.fr/>), as part of the Ssalto ground-processing segment. The  
24 Microwave OI SST data are produced by Remote Sensing Systems and sponsored by National  
25 Oceanographic Partnership Program (NOPP), the NASA Earth Science Physical  
26 Oceanography Program, and the NASA MEaSUREs DISCOVER Project. The  
27 LOCEAN\_v2013 Sea Surface Salinity maps have been produced by LOCEAN/IPSL (UMR  
28 CNRS/UPMC/IRD/MNHN) laboratory that participates to the Ocean Salinity Expertise  
29 Center (CECOS) of Centre Aval de Traitement des Données SMOS (CATDS). This  
30 product is distributed by the Ocean Salinity Expertise Center (CECOS) of the CNES-  
31 IFREMER Centre Aval de Traitement des Données SMOS (CATDS), at IFREMER,  
32 Plouzané (France). The NOCS Surface Flux Dataset v2.0 is distributed from the US National  
33 Center for Atmospheric Research (NCAR) and the British Atmospheric Data Centre (BADC).

Florian Schütte 26.4.16 10:27

**Gelöscht:** We thank the captains and crew of the research vessels as well as our technical group for their help with the fieldwork. Furthermore the authors thank Ping Chang, Rebecca Hummels and Robert Kopte for helpful discussions. We

- 1 The observations used to construct the NOC Surface Flux Dataset come from the
- 2 International Comprehensive Ocean – Atmosphere Data Set (ICOADS).
- 3

1 **Tables**

2 **Table 1:** Data from the following research cruises were used.

<b>Cruise</b>	<b>Ship</b>	<b>Time</b>	<b>Region</b>	<b>No. of Profiles</b>
Pos 320	Poseidon	March-April 2005	TANWA East	38
M 68/2	Meteor	July 2006	23°W Section	10
M 68/3	Meteor	July-August 2006	18°N Section	81
Pos 347	Poseidon	January-February 2007	TANWA East	125
Pos 348	Poseidon	February 2007	TANWA East	32
Ata 3	L'Atalante	February 2008	TANWA East	58
Ata 4	L'Atalante	March 2008	23°W Section	6
MSM 8	Maria S. Merian	May 2008	South TANWA	3
MSM 10	Maria S. Merian	December 2008	South TANWA	5
Pos 399	Poseidon	May-July 2009	TANWA East	21
M 80/1	Meteor	November 2009	23°W Section	9
M 80/2	Meteor	December 2009	South TANWA	8
M 81/1	Meteor	May 2010	Central TANWA	12
M 83/1	Meteor	December 2010	14.5°N Section	27
MSM 18/2	Maria S. Merian	May 2011	23°W Section	6
MSM 18/3	Maria S. Merian	June 2011	South TANWA	6
MSM 22	Maria S. Merian	November 2012	18°N Section	76
MSM 23	Maria S. Merian	November 2012	14.5°N Section	13
M 96	Meteor	May 2013	14.5°N Section	14
M 97	Meteor	June 2013	14.5°N Section	7
				Σ 557



1 **Table 2:** Mean properties of anticyclones, cyclones and ACMEs in the region of 12°N - 22°N, 16°W - 26°W  
 2 (TANWA) and their standard deviation given in brackets, detected from the OW-method and the GEO-method  
 3 (detectable longer than one week and with a radius >45 km). Coastal area is defined as an ~ 250km wide  
 4 corridor near the coast (see Figure 7). \*Note, that the properties of ACMEs are based on less years of SLA data  
 5 (1998-2013), due to the not available SST data.

Florian Schütte 22.4.16 14:41  
 Gelöscht: 'S  
 Florian Schütte 22.4.16 14:41  
 Gelöscht: or  
 Florian Schütte 25.4.16 17:27  
 Gelöscht: 40  
 Florian Schütte 22.4.16 14:42  
 Gelöscht: '

Florian Schütte 22.4.16 14:43  
 Gelöscht: '  
 Florian Schütte 22.4.16 14:43  
 Gelöscht: '

Property (based on SLA data between 95-2013)	OW-method			GEO-method		
	2741 [144/year]			2816 [148/year]		
	Anticyclones	Cyclones	ACMEs*	Anticyclones	Cyclones	ACMEs*
Detected eddies	1041 (38%)	1443 (53%)	257 (9%)	1137 (40%)	1422 (51%)	257 (9%)
Detected eddies in coastal area	186 [10/year]	241 [13/year]	43 [2/year]	178 [9/year]	199 [10/year]	44 [3/year]
Average lifetime [days]	30 [±31] max 282	24 [±22] max 176	26 [±28] max 197	32 [±32] max 277	27 [±29] max 180	26 [±28] max 175
Average radius [km]	53 [±5]	51 [±5]	52 [±5]	60 [±20]	62 [±22]	59 [±20]
Average westward propagation [km d <sup>-1</sup> ]	2.8(±2.4)	2.7(±2.4)	2.8(±2.5)	3.3(±1.8)	3.1(±1.9)	3.3(±1.9)

1 **Table 3: Temperature and salinity anomalies of cyclones and anticyclones vertically averaged in the upper 350**  
 2 **m. Anomaly profiles are calculated relative to different reference datasets: 1.) the nearest in-situ profile in time**  
 3 **and space, 2.) the CSIRO CARS2009a V1.1 climatology, 3.) the monthly WOA09 climatology, 4.) the monthly**  
 4 **MIMOC V2.2 climatology, 5.) the monthly Levitus94 climatology (salt values are not included in monthly**  
 5 **base).**

	Cyclones		Anticyclones	
	Temp [°C]	Salt	Temp [°C]	Salt
<b>1.) Next profile outside</b>	-1.22	-0.26	0.87	0.13
<b>2.) CSIRO</b>	-0.21	-0.08	0.94	0.06
<b>3.) WOA</b>	-0.32	-0.10	0.85	0.05
<b>4.) MIMOC</b>	-0.56	-0.32	0.60	-0.17
<b>5.) Levitus</b>	-0.16		0.97	

Florian Schütte 25.4.16 17:23

**Gelöscht:** Different mean temperature and salinity anomalies of cyclones and anticyclones (anticyclones + ACMEs) of the first 350m by removing different mean states. They are computed by removing the 1.) nearest in-situ profile in time and space, 2.) CSIRO CARS2009a V1.1 climatology, 3.) monthly WOA09 climatology, 4.) monthly MIMOC V2.2 climatology, 5.) monthly Levitus94 climatology (salt values are not included in monthly base).

Florian Schütte 25.4.16 17:23

**Gelöscht: ic eddies**

1 **Table 4:** Total available heat anomaly ( $AHA_{total}$ ) and total available salt anomaly ( $ASA_{total}$ ) of the composite  
 2 cyclones, anticyclones and ACMEs as well as contribution of a single eddy to the annual heat and salt transport  
 3 and its mean volume.  
 4

	<b>Cyclones</b>	<b>Anticyclones</b>	<b>ACMEs</b>
<b>AHA<sub>total</sub></b> [x 10 <sup>18</sup> J]	-14.5	11.0	-15.4
<b>ASA<sub>total</sub></b> [x 10 <sup>10</sup> kg]	-73.0	40.7	-94.2
<b>Heat transport</b> [x 10 <sup>11</sup> W]	-4.6	3.5	-4.9
<b>Salt transport</b> [x 10 <sup>3</sup> kg s <sup>-1</sup> ]	-23.2	12.9	-29.9
<b>Volume</b> [x 10 <sup>10</sup> m <sup>3</sup> ]	286.0	308.9	297.3

# 1 Figures

2 **Figure 1:** Schematic of the current system of the eastern tropical North Atlantic (red arrows; [North Equatorial](#)  
3 [Current \(NEC\)](#), [Canary Current \(CC\)](#), [Poleward Under Current \(PUC\)](#), [Mauretania Current \(MC\)](#), [north](#)  
4 [Equatorial Counter Current \(nNECC\)](#), [Guinea Current \(GC\)](#), [North Equatorial Under Current \(NEUC\)\)](#)) **a)** in  
5 boreal spring and **b)** in boreal autumn. Black Arrows are mean wind vectors, green areas indicate seasonal mean  
6 SST<21°C. Blue colours represent topography and the dashed box indicates the TANWA area. The mean  
7 position of the [Intertropical Convergence Zone \(ITCZ\)](#) in autumn is indicated by the two black dashed lines in  
8 **b)**.

Florian Schütte 1.4.16 15:04

**Formatiert:** Schriftart:10 pt, Nicht Fett,  
Schriftfarbe: Automatisch

9 **Figure 2:** Mean salinity **(a)** and potential temperature **(b)** at 100 m depth in the TANWA from the MIMOC  
10 Climatology (Schmidtke et al., 2013) and  $\Theta/S$  diagram **(c)**. The thick black/white line in **a)** and **b)** indicates the  
11 CVFZ. In **a)** crosses and dots represent all available profiles (from Argo floats and ships) in the marked coastal  
12 and offshore boxes, respectively. In **b)**, the thin dashed line mark cruise tracks of 20 research cruises to the  
13 TANWA taking profiles used in the present study. The black cross in **b)** indicates the position of the Cape Verde  
14 Ocean Observatory (CVOO) mooring. In **c)** data from the coastal and offshore boxes are marked by crosses and  
15 dots, respectively; superimposed are isolines of potential density.

16 **Figure 3:** Locations of available profiles obtained in the TANWA between 1995 and 2013. Red dots mark  
17 shipboard CTD stations, blue dots locations of Argo float profiles and the black cross the location of the CVOO  
18 mooring.

Florian Schütte 5.4.16 14:46

**Gelöscht:** and

19 **Figure 4:** Snapshot of the SLA for Dec. 22, 2010, with the results of the eddy-detection methods: OW-Method  
20 (solid white line) and the GEO-Method (dashed white line) with geostrophic velocities superimposed (black  
21 arrows). The black dots mark Argo float profiles, the white cross in **a)** indicates the CVOO mooring. In **a)** SLA  
22 in the TANWA is shown and in **b)** a zoom of a selected region with a cyclonic eddy.

23 **Figure 5:** Location of all profiles taken in **a)** cyclones, **b)** anticyclones, **c)** ACMEs and **d)** outside of an eddy.

24 **Figure 6:** Number of eddies against lifetime in days from the OW-method (left) and GEO-method (right).  
25 Percentage of ACMEs, anticyclones (Ant) and cyclones (Cyc) is given in the tables on the right and left.

26 **Figure 7:** Total numbers of eddies generated within  $1^\circ \times 1^\circ$  boxes (colors) [based on the results of the OW-](#)  
27 [method](#). Marked are the headlands Cap Timris (Mauretania), Saint-Louis (Senegal), Cap Vert (Senegal) and the  
28 Islands Santo Antão (Cape Verde) and Fogo (Cape Verde), which can be associated with the most productive  
29 eddy generating regions. The thick solid black line along  $18^\circ W/19^\circ W$  separates the coastal region from the  
30 offshore region.

31 **Figure 8:** Number of eddies generated in  $1^\circ \times 1^\circ$  boxes **(a, c, e)** and total number of eddies detected in  $1/6^\circ \times$   
32  $1/6^\circ$  boxes [based on the results of the OW-method](#) **(b, d, f)** for cyclones **(a, b)**, anticyclones **(c, d)** and  
33 ACMEs **(e, f)**. In **b), d)** and **f)** only eddies are counted with a lifetime larger than 35 days. In **b), d)**, and **f)** main  
34 eddy propagation corridors are indicated by [straight gray lines](#); [black lines show trajectories of long-lived eddies](#)  
35 [with a lifetime larger than 150 days](#). The thick solid black line along  $18^\circ W/19^\circ W$  in **a), c)** and **e)** separates the  
36 coastal region from the offshore region.

Florian Schütte 25.4.16 17:24

**Gelöscht:** solid

Florian Schütte 25.4.16 17:25

**Gelöscht:** black

Florian Schütte 25.4.16 17:25

**Gelöscht:** and thick black arrows, main  
generation spots by circles with crosses.

Florian Schütte 5.4.16 11:50

**Gelöscht:**

37 **Figure 9:** Seasonal cycle of the number of newly detected eddies per year [based on the results of the OW-](#)  
38 [method](#) in the coastal region as shown in Figures 7 and 8. In **a)** all eddies are marked by the black line,  
39 cyclones by the blue line and all anticyclonic eddies by the orange line. In **b)** anticyclonic eddies are separated  
40 into anticyclones (red line) and ACMEs (green line). The shaded areas around the lines represent the standard  
41 error.

1 **Figure 10:** Phase of the annual harmonic of the number of detected eddies in  $2^\circ \times 2^\circ$  boxes [based on the](#)  
2 [results of the OW-method](#) for **a)** cyclones and **b)** anticyclones. Phases are only shown for boxes with an  
3 amplitude larger than 2.5 eddies. Phase is given in month of the year with maximum eddy number.

4 **Figure 11:** Composites of SLA, SST and SSS [anomalies](#) of a cyclone, anticyclone and ACME in [the](#) TANWA  
5 [based on the results of the OW-method](#). Composite SLA for each eddy type and the associated geostrophic  
6 velocity (white arrows) are shown in **a)**, **b)** and **c)**; SST [anomaly](#) in **d)**, **e)** and **f)**; and SSS [anomaly](#) in **g)**, **h)** and  
7 **i)**, respectively. The solid circles mark the mean eddy radius.

8 **Figure 12:** Vertical structure of the composite cyclone, anticyclone and ACME in [the](#) TANWA as presented as  
9 sections across the eddies (left three columns) and mean profiles (right column). In **a)** potential temperature, in  
10 **b)** salinity and in **c)** potential density anomaly relative to the nearest profile outside of the eddy is shown. [Black](#)  
11 [contour lines](#) in the left three columns mark mean [isotherms](#), [isohalines](#) and [isopycnal](#) surfaces. In the right  
12 column, solid lines represent the composite ACME, dashed lines the anticyclone and dashed-dot lines the  
13 cyclone; the error bars at the black dots represent the standard deviation calculated from the individual anomaly  
14 profiles.

15 **Figure 13:** Mean profiles of available **a)** heat and **b)** salt anomaly per meter of the composite cyclone (blue line),  
16 anticyclone (red line) and ACME (green line).

17 **Figure 14:** **a)** Map of [the](#) TANWA divided into three areas (Area I: the extended boundary current region, Area  
18 II: the transition zone, and Area III: the subtropical gyre region). Number inside of the boxes are the number of  
19 eddies (blue-cyclones, red-anticyclones, green-ACMEs), which are generated (star), cease (cross) and  
20 propagating from one area into another (arrow). **b)** Annual mean net heat flux from NOC Surface Flux Dataset  
21 (colors) with three areas marked. Black numbers are the mean net heat flux ( $\overline{Hf\bar{x}}$ ) in the corresponding area. The  
22 table includes the eddy type dependent (blue: cyclones, red: anticyclones, green: ACMEs) heat and salt release in  
23 Area II.

24 **Figure 15:** Vertical sections of SACW anomaly relative to the surrounding water across the composite cyclone  
25 (left), anticyclone (middle) and ACME (right) in [the](#) TANWA.

26 **Figure 16:** **a)**  $S-\sigma_\theta$  diagram with thick and thin black lines indicating mean and standard deviation, respectively,  
27 of characteristic SACW and NACW properties derived from the ensemble of profiles taken in [the](#) TANWA  
28 (grey lines). Mean eddy dependent watermass properties are given for cyclones (blue line), anticyclones (red  
29 line) and ACMEs (green line). **b)** Percentage of SACW in the upper 350m as shown for all available profiles  
30 (color) and as mean numbers for the three regions: the extended boundary current region (Area I), the transition  
31 zone (Area II) and the subtropical gyre region (Area III) that are separated by black straight lines. Numbers in  
32 the white circles are the mean percentage of SACW of the composite cyclones (blue), anticyclones (red) and  
33 ACMEs (green) in the corresponding areas. The eddy transport of SACW from the boundary current into Area I,  
34 from Area I into Area II and from Area II into Area III is marked by thick black arrows with transport numbers  
35 in Sv given in the white boxes for composite cyclones (blue), anticyclones (red), ACMEs (green) and total  
36 transport (black).

Florian Schütte 11.4.16 15:25

Gelöscht: C

Florian Schütte 11.4.16 15:25

Gelöscht: potential density

Florian Schütte 22.4.16 14:47

Gelöscht: '

Florian Schütte 22.4.16 14:47

Gelöscht: '

1  
2  
3  
4  
5  
6  
7  
8  
9  
10  
11  
12  
13  
14  
15  
16  
17  
18  
19  
20  
21  
22  
23  
24  
25  
26  
27  
28  
29  
30  
31  
32  
33  
34  
35  
36  
37

## References

- Alpers, W., Brandt, P., Lazar, A., Dagorne, D., Sow, B., Faye, S., Hansen, M. W., Rubino, A., Poulain, P.-M., and Brehmer, P.: A small-scale oceanic eddy off the coast of West Africa studied by multi-sensor satellite and surface drifter data, *Remote Sensing of Environment*, 129, 132-143, 2013.
- Barton, E.: Meanders, eddies and intrusions in the thermohaline front off Northwest Africa, *Oceanol Acta*, 10, 267-283, 1987.
- Barton, E. D.: The Poleward Undercurrent on the Eastern Boundary of the Subtropical North Atlantic. In: *Poleward Flows Along Eastern Ocean Boundaries*, Neshyba, S. J., Mooers, C. N. K., Smith, R. L., and Barber, R. T. (Eds.), Coastal and Estuarine Studies, Springer New York, 82-95, 1989.
- Berry, D. I. and Kent, E. C.: Air–Sea fluxes from ICOADS: the construction of a new gridded dataset with uncertainty estimates, *International Journal of Climatology*, 31, 987-1001, 2011.
- Boutin, J., Martin, N., Reverdin, G., Yin, X., and Gaillard, F.: Sea surface freshening inferred from SMOS and ARGO salinity: Impact of rain, *Ocean Sci*, 9, 183-192, 2013.
- Brandt, P., Bange, H. W., Banyte, D., Dengler, M., Didwischus, S. H., Fischer, T., Greatbatch, R. J., Hahn, J., Kanzow, T., Karstensen, J., Körtzinger, A., Krahnemann, G., Schmidtko, S., Stramma, L., Tanhua, T., and Visbeck, M.: On the role of circulation and mixing in the ventilation of oxygen minimum zones with a focus on the eastern tropical North Atlantic, *Biogeosciences*, 12, 489-512, 2015.
- Chaigneau, A., Eldin, G., and Dewitte, B.: Eddy activity in the four major upwelling systems from satellite altimetry (1992–2007), *Progress in Oceanography*, 83, 117-123, 2009.
- Chaigneau, A., Gizolme, A., and Grados, C.: Mesoscale eddies off Peru in altimeter records: Identification algorithms and eddy spatio-temporal patterns, *Progress in Oceanography*, 79, 106-119, 2008.
- Chaigneau, A., Le Texier, M., Eldin, G., Grados, C., and Pizarro, O.: Vertical structure of mesoscale eddies in the eastern South Pacific Ocean: A composite analysis from altimetry and Argo profiling floats, *Journal of Geophysical Research: Oceans*, 116, C11025, doi:10.1029/2011JC007134, 2011.
- Chang, C.-H., Xie, S.-P., Schneider, N., Qiu, B., Small, J., Zhuang, W., Taguchi, B., Sasaki, H., and Lin, X.: East Pacific ocean eddies and their relationship to subseasonal variability in Central American wind jets, *Journal of Geophysical Research: Oceans*, 117, C10001, doi:10.1029/2011JC007315, 2012.

- 1 Chelton, D. B., deSzoeki, R. A., Schlax, M. G., El Naggar, K., and Siwertz, N.: Geographical  
2 Variability of the First Baroclinic Rossby Radius of Deformation, *Journal of Physical*  
3 *Oceanography*, 28, 433-460, 1998.
- 4 Chelton, D. B., Schlax, M. G., and Samelson, R. M.: Global observations of nonlinear  
5 mesoscale eddies, *Progress in Oceanography*, 91, 167-216, 2011.
- 6 Chelton, D. B., Schlax, M. G., Samelson, R. M., and de Szoeki, R. A.: Global observations of  
7 large oceanic eddies, *Geophysical Research Letters*, 34, L15606,  
8 doi:10.1029/2007GL030812, 2007.
- 9 Crawford, W., Cherniawsky, J., Foreman, M., and Gower, J.: Formation of the Haida -  
10 1998 oceanic eddy, *Journal of Geophysical Research: Oceans* (1978–2012), 107, 6-1-6-  
11 11, 2002.
- 12 [Cushman Roisin B. and Tang B.: Geostrophic Turbulence and Emergence of Eddies](#)  
13 [beyond the Radius of Deformation, \*Journal of Physical Oceanography\*, 20, 97–113, doi:](#)  
14 [10.1175/15200485\(1990\)020<0097:GTAEOE>2.0.CO;2, 1990](#)
- 15
- 16 Cushman-Roisin, B., Tang, B., and Chassignet, E. P.: Westward Motion of Mesoscale  
17 Eddies, *Journal of Physical Oceanography*, 20, 758-768, 1990.
- 18 de Boyer Montégut, C., Madec, G., Fischer, A. S., Lazar, A., and Iudicone, D.: Mixed layer  
19 depth over the global ocean: An examination of profile data and a profile-based  
20 climatology, *Journal of Geophysical Research: Oceans*, 109, C12003,  
21 doi:10.1029/2004JC002378, 2004.
- 22 Fu, L.-L. and Ferrari, R.: Observing Oceanic Submesoscale Processes From Space, *Eos*,  
23 *Transactions American Geophysical Union*, 89, 488-488, 2008.
- 24 Garzoli, S. L. and Katz, E. J.: The Forced Annual Reversal of the Atlantic North Equatorial  
25 Countercurrent, *Journal of Physical Oceanography*, 13, 2082-2090, 1983.
- 26 Glessmer, M. S., Eden, C., and Oschlies, A.: Contribution of oxygen minimum zone waters  
27 to the coastal upwelling off Mauritania, *Progress in Oceanography*, 83, 143-150, 2009.
- 28 Hagen, E.: A meandering intermediate front North-West off Cape Verde islands, 1985.  
29 *Oceanogr. Trop.*, 20: 71-83, 1985.
- 30 [Hood, E.M.C, L. Sabine and B.M. Sloyan: The GO-SHIP repeat hydrography manual: A](#)  
31 [collection of expert reports and guidelines, IOCCP Rep 14, 2010](#)
- 32 [Hughes P. and E. D. Barton: Stratification and water mass structure in the upwelling area](#)  
33 [off Northwest Africa in April/May 1969, \*Deep-Sea Research\*, 21, 6111-628, 1974](#)

Florian Schütte 11.4.16 17:23

Formatiert: Schriftart: Cambria

Florian Schütte 11.4.16 17:23

Formatiert: Schriftart: Cambria

Florian Schütte 11.4.16 17:23

Formatiert: Schriftart: Cambria

1 Isern-Fontanet, J., García-Ladona, E., and Font, J.: Vortices of the Mediterranean Sea: An  
2 Altimetric Perspective, *Journal of Physical Oceanography*, 36, 87-103, 2006.

3 Johns, W. E., Zantopp, R. J., and Goni, G. J.: Cross-gyre transport by North Brazil Current  
4 rings, *Elsevier Oceanography Series*, 68, 411-441, 2003.

5 [Jones, P. G. W. and A. R. Folkard: Chemical oceanographical observations off the coast of  
6 North-West Africa, with special reference to the process of upwelling, \*Rapports et  
7 proc~s verbaux du Conseil International pour l'Exploration de la Mer\* 159, 38-60, 1970](#)  
8

9 Karstensen, J., Fiedler, B., Schütte, F., Brandt, P., Körtzinger, A., Fischer, G., Zantopp, R.,  
10 Hahn, J., Visbeck, M., and Wallace, D.: Open ocean dead zones in the tropical North  
11 Atlantic Ocean, *Biogeosciences*, 12, 2597-2605, 2015.

12 Klinger, B. A.: Baroclinic eddy generation at a sharp corner in a rotating system, *Journal*  
13 *of Geophysical Research: Oceans* (1978–2012), 99, 12515-12531, 1994a.

14 Klinger, B. A.: Inviscid Current Separation from Rounded Capes, *Journal of Physical*  
15 *Oceanography*, 24, 1805-1811, 1994b.

16 Kostianoy, A. G. and Belkin, I. M.: A Survey of Observations on Emtrathermocline Eddies  
17 in the World Ocean. In: *Elsevier Oceanography Series*, Nihoul, J. C. J. and Jamart, B. M.  
18 (Eds.), Elsevier, 1989.

19 Kurczyn, J., Beier, E., Lavín, M., and Chaigneau, A.: Mesoscale eddies in the northeastern  
20 Pacific tropical - subtropical transition zone: Statistical characterization from satellite  
21 altimetry, *Journal of Geophysical Research: Oceans* (1978–2012), 117, C10021,  
22 doi:10.1029/2012JC007970, 2012.

23 Kurian, J., Colas, F., Capet, X., McWilliams, J. C., and Chelton, D. B.: Eddy properties in the  
24 California current system, *Journal of Geophysical Research: Oceans* (1978–2012), 116,  
25 C08027, doi:10.1029/2010JC006895, 2011.

26 Lázaro, C., Fernandes, M. J., Santos, A. M. P., and Oliveira, P.: Seasonal and interannual  
27 variability of surface circulation in the Cape Verde region from 8 years of merged T/P  
28 and ERS-2 altimeter data, *Remote Sensing of Environment*, 98, 45-62, 2005.

29 Liang, J.-H., McWilliams, J. C., Kurian, J., Colas, F., Wang, P., and Uchiyama, Y.: Mesoscale  
30 variability in the northeastern tropical Pacific: Forcing mechanisms and eddy properties,  
31 *Journal of Geophysical Research: Oceans*, 117, C07003, doi: 10.1029/2012JC008008,  
32 2012.

33 [Liu Y., C. Dong, Y. Guan, D. Chen, J. McWilliams, F. Nencioli: Eddy analysis in the  
34 subtropical zonal band of the North Pacific Ocean, \*Deep Sea Research Part I:  
35 Oceanographic Research Papers\*, Volume 68, Pages 54-67, ISSN 0967-0637,  
36 <http://dx.doi.org/10.1016/j.dsr.2012.06.001>, 2012.](#)

Florian Schütte 12.4.16 08:33

Formatiert: Schriftart: Cambria

Florian Schütte 11.4.16 17:17

Formatiert: Schriftart: Cambria

Florian Schütte 11.4.16 17:17

Formatiert: Schriftart: Cambria

Florian Schütte 11.4.16 17:17

Formatiert: Schriftart: Cambria

Florian Schütte 11.4.16 17:17

Formatiert: Schriftart: Cambria

Florian Schütte 11.4.16 17:17

Formatiert: Schriftart: Cambria

Florian Schütte 11.4.16 17:17

Formatiert: Schriftart: Cambria

Florian Schütte 11.4.16 17:17

Formatiert: Schriftart: Cambria



- 1
- 2 Luyten, J. R., Pedlosky, J., and Stommel, H.: The ventilated thermocline, *Journal of*  
3 *Physical Oceanography*, 13, 292-309, 1983.
- 4 Mittelstaedt, E.: The ocean boundary along the Northwest African Coast - circulation and  
5 oceanographic properties at the sea-surface, *Progress in Oceanography*, 26, 307-355,  
6 1991.
- 7 Mittelstaedt, E.: The upwelling area off Northwest Africa - a description of phenomena  
8 related to coastal upwelling, *Progress in Oceanography*, 12, 307-331, 1983.
- 9 Nencioli, F., Dong, C., Dickey, T., Washburn, L., and McWilliams, J. C.: A Vector Geometry-  
10 Based Eddy Detection Algorithm and Its Application to a High-Resolution Numerical  
11 Model Product and High-Frequency Radar Surface Velocities in the Southern California  
12 Bight, *J Atmos Ocean Tech*, 27, 564-579, 2010.
- 13 Okubo, A.: Horizontal dispersion of floatable particles in the vicinity of velocity  
14 singularities such as convergences, *Deep Sea Research and Oceanographic Abstracts*, 17,  
15 445-454, 1970.
- 16 Ould-Dedah, S., Wiseman Jr, W. J., and Shaw, R. F.: Spatial and temporal trends of sea  
17 surface temperature in the northwest African region, *Oceanol Acta*, 22, 265-279, 1999.
- 18 Pantoja, D., Marinone, S., Parés-Sierra, A., and Gómez-Valdivia, F.: Numerical modeling of  
19 seasonal and mesoscale hydrography and circulation in the Mexican Central Pacific  
20 Modelación numérica de la hidrografía y circulación estacional y de mesoescala en el  
21 Pacífico central mexicano, *Ciencias Marinas*, 38, 363-379, 2012.
- 22 Pares-Sierra, A., White, W. B., and Tai, C. K.: Wind-driven Coastal Generation of Annual  
23 Mesoscale Eddy Activity in the California Current, *Journal of Physical Oceanography*, 23,  
24 1110-1121, 1993.
- 25 Pastor, M. V., Pelegrí, J. L., Hernández-Guerra, A., Font, J., Salat, J., and Emelianov, M.:  
26 Water and nutrient fluxes off Northwest Africa, *Continental Shelf Research*, 28, 915-936,  
27 2008.
- 28 [Pegliasco C., Chaigneau A., Morrow R.: Main eddy vertical structures observed in the four](#)  
29 [major Eastern Boundary Upwelling Systems, \*Journal of Geophysical Research\*, Vol. 120,](#)  
30 [6008-6033, doi: 10.1002/2015JC01950, 2015](#)
- 31 Peña-Izquierdo, J., Pelegrí, J. L., Pastor, M. V., Castellanos, P., Emelianov, M., Gasser, M.,  
32 Salvador, J., and Vázquez-Domínguez, E.: The continental slope current system between  
33 Cape Verde and the Canary Islands, *Sci Mar*, 76, 65-78, 2012.
- 34 Peña - Izquierdo, J., van Sebille, E., Pelegrí, J. L., Sprintall, J., Mason, E., Llanillo, P. J., and  
35 Machín, F.: Water mass pathways to the North Atlantic oxygen minimum zone, *Journal of*

- 1 Geophysical Research: Oceans, vol. 120, page range 3350-3372,  
2 doi:10.1002/2014JC010557, 2015.
- 3 Pichevin, T. and Nof, D.: The eddy cannon, Deep Sea Research Part I: Oceanographic  
4 Research Papers, 43, 1475-1507, 1996.
- 5 Polonsky, A. and Artamonov, Y.: North equatorial countercurrent in the tropical Atlantic:  
6 Multi-jet structure and seasonal variability, Deutsche Hydrographische Zeitschrift, 49,  
7 477-495, 1997.
- 8 Richardson, P. L. and Reverdin, G.: Seasonal cycle of velocity in the Atlantic North  
9 Equatorial Countercurrent as measured by surface drifters, current meters, and ship  
10 drifts, Journal of Geophysical Research: Oceans, 92, 3691-3708, 1987.
- 11 Røed, L. P.: Curvature effects on hydraulically driven inertial boundary currents, J Fluid  
12 Mech, 96, 395-412, 1980.
- 13 Sangrà, P., Pascual, A., Rodríguez-Santana, Á., Machín, F., Mason, E., McWilliams, J. C.,  
14 Pelegrí, J. L., Dong, C., Rubio, A., Arístegui, J., Marrero-Díaz, Á., Hernández-Guerra, A.,  
15 Martínez-Marrero, A., and Auladell, M.: The Canary Eddy Corridor: A major pathway for  
16 long-lived eddies in the subtropical North Atlantic, Deep Sea Research Part I:  
17 Oceanographic Research Papers, 56, 2100-2114, 2009.
- 18 Schmidtko, S., Johnson, G. C., and Lyman, J. M.: MIMOC: A global monthly isopycnal  
19 upper-ocean climatology with mixed layers, Journal of Geophysical Research: Oceans,  
20 118, 1658-1672, 2013.
- 21 Siedler, G., Zangenber, N., Onken, R., and Morlière, A.: Seasonal changes in the tropical  
22 Atlantic circulation: Observation and simulation of the Guinea Dome, Journal of  
23 Geophysical Research: Oceans, 97, 703-715, 1992.
- 24 Stramma, L., Bange, H. W., Czeschel, R., Lorenzo, A., and Frank, M.: On the role of  
25 mesoscale eddies for the biological productivity and biogeochemistry in the eastern  
26 tropical Pacific Ocean off Peru, Biogeosciences, 10, 7293-7306, 2013.
- 27 Stramma, L. and Isemer, H.-J.: Seasonal variability of meridional temperature fluxes in  
28 the eastern North Atlantic Ocean, J Mar Res, 46, 281-299, 1988.
- 29 Stramma, L. and Schott, F.: The mean flow field of the tropical Atlantic Ocean, Deep Sea  
30 Research Part II: Topical Studies in Oceanography, 46, 279-303, 1999.
- 31 Stramma, L. and Siedler, G.: Seasonal changes in the North Atlantic subtropical gyre,  
32 Journal of Geophysical Research: Oceans, 93, 8111-8118, 1988.
- 33 Weiss, J.: The dynamics of enstrophy transfer in two-dimensional hydrodynamics,  
34 Physica D: Nonlinear Phenomena, 48, 273-294, 1991.

- 1 Yin, X., Boutin, J., and Spurgeon, P.: First assessment of SMOS data over open ocean: Part  
2 1—Pacific Ocean, *Geoscience and Remote Sensing, IEEE Transactions on*, 50, 1648-1661,  
3 2012.
- 4 Zamudio, L., Hurlburt, H. E., Metzger, E. J., Morey, S. L., O'Brien, J. J., Tilburg, C., and Zavala  
5 - Hidalgo, J.: Interannual variability of Tehuantepec eddies, *Journal of Geophysical*  
6 *Research: Oceans (1978–2012)*, 111, C05001, doi:10.1029/2005JC003182, 2006.
- 7 Zamudio, L., Hurlburt, H. E., Metzger, E. J., and Tilburg, C. E.: Tropical wave - induced  
8 oceanic eddies at Cabo Corrientes and the María Islands, Mexico, *Journal of Geophysical*  
9 *Research: Oceans (1978–2012)*, 112, C05048, doi:10.1029/2006JC004018, 2007.
- 10 Zamudio, L., Leonardi, A. P., Meyers, S. D., and O'Brien, J. J.: ENSO and eddies on the  
11 southwest coast of Mexico, *Geophysical Research Letters*, 28, 13-16, 2001.
- 12 Zenk, W., Klein, B., and Schroder, M.: Cape Verde Frontal Zone, *Deep Sea Research Part A.*  
13 *Oceanographic Research Papers*, 38, Supplement 1, S505-S530, 1991.
- 14 Zhang, Z., Wang, W., and Qiu, B.: Oceanic mass transport by mesoscale eddies, *Science*,  
15 345, 322-324, 2014.  
16